

**UNIVERSITY OF GAZIANTEP  
GRADUATE SCHOOL OF  
NATURAL & APPLIED SCIENCES**

**INVESTIGATION OF PROPAGATION CHARACTERISTICS OF  
A COMPOSITE MATERIAL COMPOSED OF A  
BIANISOTROPIC METAMATERIAL AND AN ISOTROPIC  
CONVENTIONAL MATERIAL**

**M. Sc. THESIS  
IN  
ELECTRICAL AND ELECTRONICS ENGINEERING**

**BY  
MUSA BUTE  
SEPTEMBER 2013**

**Investigation of Propagation Characteristics of a Composite  
Material Composed of a Bianisotropic Metamaterial and an  
Isotropic Conventional Material**

**M.Sc. Thesis**

**in**

**Electrical and Electronics Engineering**

**University of Gaziantep**

**Supervisor**

**Assoc. Prof. Dr. Uğur Cem HASAR**

**by**

**Musa BUTE**

**September 2013**

© 2013 [Musa BUTE]

REPUBLIC OF TURKEY  
UNIVERSITY OF GAZİANTEP  
GRADUATE SCHOOL OF NATURAL & APPLIED SCIENCES  
ELECTRICAL – ELECTRONICS ENGINEERING

Name of the thesis: Investigation of propagation characteristics of a composite material composed of a bianisotropic metamaterial and an isotropic conventional material.

Name of the student: Musa BUTE

Exam date: 06.09.2013

Approval of the Graduate School of Natural and Applied Sciences

  
Assoc. Prof. Dr. Metin BEDİR


Director

I certify that this thesis satisfies all the requirements as a thesis for the degree of Master of Science.

  
Prof. Dr. Celal KORAŞLI

Head of Department

This is to certify that we have read this thesis and that in our consensus opinion it is fully adequate, in scope and quality, as a thesis for the degree of Master of Science.

  
Assoc. Prof. Dr. Uğur Cem HASAR

Supervisor

Examining Committee Members

Prof. Dr. Ergün ERÇELEBİ (Chairman)



Assoc. Prof. Dr. Uğur Cem HASAR



Assoc. Prof. Dr. Gökhan APAYDIN



**I hereby declare that all information in this document has been obtained and presented in accordance with academic rules and ethical conduct. I also declare that, as required by these rules and conduct, I have fully cited and referenced all material and results that are not original to this work.**

Musa BUTE

## **ABSTRACT**

### **INVESTIGATION OF PROPAGATION CHARACTERISTICS OF A COMPOSITE MATERIAL COMPOSED OF A BIANISOTROPIC METAMATERIAL AND AN ISOTROPIC CONVENTIONAL MATERIAL**

BUTE, Musa

M.Sc. in Electrical and Electronics Eng.

Supervisor: Assoc. Prof. Dr. Uğur Cem HASAR

September 2013, 84 pages

It is well-known that metamaterials fabricated by an engineering design possess electromagnetic properties unavailable in conventional materials such as negative refractive index and perfect lens. Within the broad scope of metamaterials, bi-anisotropic metamaterials have properties different than isotropic metamaterials in that they have different forward and backward wave impedances, different forward and backward reflection scattering parameters, a wider stop-band compared to isotropic metamaterials, and a magneto-electric coupling coefficient. In the literature, wave propagation characteristics of different composite metamaterial media are investigated. To our best knowledge, wave propagation characteristics of a composite structure comprising of a bi-anisotropic metamaterial slab and an isotropic conventional slab has not yet been analyzed. In this thesis, propagation characteristics of the aforementioned structure is investigated. In the purpose of this thesis, we analytically derived forward and backward reflection and transmission scattering parameters of the composite structure, for a uniform plane wave incident normally to the composite medium. Moreover, analytically derived parameters are validated by a numerical analysis. Finally, after derivation and validation of scattering parameters, we analyzed the wave characteristics of the composite structure fabricated by only split ring resonators using a commercially available electromagnetic/microwave simulation software package (CST Microwave Studio).

**Key Words:** Metamaterials, Bianisotropy, Scattering Parameters, Composite Structures, CST.

## ÖZET

### İZOTROPİK KONVENSİYONEL BİR MALZEME İLE BİANİZOTROPİK BİR METAMALZEMEDEN OLUŞAN KOMPOZİT BİR YAPININ YAYILIM KARAKTERİSTİĞİNİN ANALİZİ

BUTE, Musa

Yüksek Lisans Tezi, Elektrik-Elektronik Müh. Bölümü

Tez Yöneticisi: Doç. Dr. Uğur Cem HASAR

Eylül 2013, 84 sayfa

Bilindiği üzere metamalzemeler, normal malzemelerde bulunmayan negatif kırılma indisi ve mükemmel lens gibi elektromanyetik özellikleri mühendislik tasarımları kazandırılarak üretilmektedir. Metamalzemenin geniş kapsama alanı içerisinde, bianizotropik metamalzemeler ileri-geri empedans ve yansıma saçılma parametrelerinin farklılık göstermesi ve kuplaj katsayısına sahip olması nedeniyle normal metamalzemelerden farklı özellikler göstermektedir. Bildiğimiz kadarıyla literatürde, bianizotropik bir metamalzeme ve normal malzemedен oluşan bir kompozit yapının elektromanyetik dalga yayılım karakteristiğini henüz inceleyen olmamıştır. Bu tezde, yukarıda bahsedilen kompozit yapının yayılım karakteristiği incelenmiştir. Bu amaç doğrultusunda bu kompozit yapının analitik olarak ileri-geri yansıma ve iletim saçılma parametreleri normal düzlemsel gelen dalga modeli ile bulunmuştur. Bununla birlikte bulunan parametreler nümerik analiz olarak da doğrulanmıştır. Son olarak, saçılma parametrelerinin bulunması ve doğrulanmasından sonra yarık halka rezonatör yapı ile bu kompozit yapının dalga yayılım karakteristiği elektromanyetik yazılım simülasyon programı olan CST mikrodalga kütüphanesi ile de analiz edilerek desteklenmiştir.

**Anahtar Kelimeler:** Metamalzemeler, Bianizotropi, Saçılma Parametreleri, Kompozit yapılar, CST.

*“To my family”*



## **ACKNOWLEDGEMENTS**

Firstly, I would like to express my best wishes to my supervisor Assoc. Prof. Dr. Uğur Cem HASAR, and also my ex-supervisors Prof. Dr. Celal KORAŞLI and Prof. Dr. Savaş UÇKUN for their guidance, advice, criticism, encouragements, and understandings throughout this study.

Special thanks to my friends, Mehmet Emin VURAL, Fuat BAŞANALAN and Mehmet Şerif DALGIÇ for their kind help, encouragement, and patience during my study.

Finally, I also wish to thank most sincerely to my family for their patience and help.

## TABLE OF CONTENTS

ABSTRACT.....	V
ÖZET.....	VI
ACKNOWLEDGEMENTS.....	VIII
TABLE OF CONTENTS.....	IX
LIST OF FIGURES.....	XI
LIST OF SYMBOLS /ABBREVIATIONS.....	XIII
CHAPTER I (INTRODUCTION) .....	1
1.1. Background.....	1
1.2. Literature Review.....	2
1.2.1 Isotropic Metamaterial.....	2
1.2.2 Bi-anisotropic metamaterials.....	3
1.3 Motivation of the Thesis.....	4
CHAPTER II (THEORETICAL ANALYSIS ) .....	6
2.1 Introduction.....	6
2.2 General Field Expressions of a Bi-anisotropic Metamaterial Slab.....	7
2.3 Forward and Backward Reflection and Transmission Scattering Parameters .....	13
2.3.1 Forward Reflection and Transmission Scattering Parameters.....	13
2.3.1.1 Derivation of Forward Reflection Scattering Parameter.....	16
2.3.1.2 Derivation of Forward Transmission Scattering Parameter....	18
2.3.2 Backward Reflection and Transmission Scattering Parameter.....	21
2.3.2.1 Derivation of Backward Reflection Scattering Parameter.....	22
2.3.2.2 Derivation of Backward Transmission Scattering Parameter.	24
2.4 Power Analysis.....	27
CHAPTER III (NUMERICAL ANALYSIS) .....	35
3.1 Introduction.....	35
3.2 Lorentz Model.....	36
3.3 Transfer Matrix Method.....	37

3.4 Validation of S-Parameters by Transfer Matrix Method (TMM) and Lorentzian Model.....	40
3.4.1 Validation of $S_{11}$ .....	41
3.4.2 Validation of $S_{21}$ .....	42
3.4.3 Validation of $S_{12}$ .....	43
3.4.4 Validation of $S_{22}$ .....	44
3.5 Power Analysis.....	45
3.5.1 Low – Loss Case.....	45
3.5.2 Lossy Case.....	49
CHAPTER IV (SIMULATION RESULTS) .....	52
4.1 Introduction.....	52
4.2 Analysis of the Isotropic Slab in CST.....	53
4.3 Analysis of the Bianisotropic Slab in CST.....	56
4.4 Analysis of Composite Structure in CST.....	58
CHAPTER V (CONCLUSION) .....	60
5.1 Results .....	60
5.2 Future Work.....	61
REFERENCES.....	62
APPENDIX.....	67

## LIST OF FIGURES

Figure 2.1: Composite structure composed of bi-anisotropic and isotropic slab ( The problem under investigation ) .....	7
Figure 2.2: Analysis of composite structure in a forward direction.....	14
Figure 2.3: Analysis of composite structure in a backward direction.....	21
Figure 3.1: Dependencies of magnitudes and phases of forward reflection scattering parameter $S_{11}$ .....	41
Figure 3.2: Dependencies of magnitudes and phases of forward reflection scattering parameter $S_{21}$ .....	42
Figure 3.3: Dependencies of magnitudes and phases of forward reflection scattering parameter $S_{12}$ .....	43
Figure 3.4: Dependencies of magnitudes and phases of forward reflection scattering parameter $S_{22}$ .....	44
Figure 3.5: Dependencies of a) and b) reflected powers, c) and d) transmitted powers, e) and f) loss powers of the two-layer composite structure ( $L_1=L_2=10$ .mm ).....	46
Figure 3.6: Dependencies of a) and b) reflected powers, c) and d) transmitted powers, e) and f) loss powers of the two-layer composite structure ( $L_1=40$ .mm, $L_2=10$ .mm ) .....	48
Figure 3.7: Dependencies of a) and b) reflected powers, c) and d) transmitted powers, e) and f) loss powers of the two-layer composite structure ( $L_1= L_2=10$ .mm ) .....	50

Figure 3.8: Dependencies of a) and b) reflected powers, c) and d) transmitted powers, e) and f) loss powers of the two-layer composite structure ( $L_1=40$ .mm, $L_2=10$ .mm).....	51
Figure 4.1: Schematic of a split-ring resonator used to construct metamaterials. When a plane wave polarized along the z-axis is incident in the x direction, the metamaterial shows bi-anisotropy. ....	53
Figure 4.2: Simulation of isotropic slab in CST program.....	54
Figure 4.3: Magnitude and phase of the forward(backward) transmission(reflection) constants of the isotropic slab. ....	55
Figure 4.4: Simulation of bianisotropic slab in CST program.....	56
Figure 4.5: Magnitude and phase of the forward (backward) transmission (reflection) constants of the bianisotropic slab. ....	57
Figure 4. 6: The problem under investigation in CST program.....	58
Figure 4. 7: Magnitude and phase of the forward(backward) transmission(reflection) constants of the composite structure. ....	58

## LIST OF SYMBOLS/ABBREVIATIONS

$\vec{B}$	Magnetic Flux Density
$c$	Speed of Light in Free Space
$\vec{D}$	Electric Flux Density
$\vec{E}$	Electric Field Intensity
$f$	Frequency
$\vec{H}$	Magnetic Field Intensity
$k$	Wave Propagation Constant
$n$	Refractive Index
$S$	Scattering Parameter
$\vec{S}$	Poynting Vector
$v$	Speed of Plane Wave In Medium
$Y$	Admittance
$Z$	Wave Impedance
$Z_0$	Characteristic Impedance
$z^+$	Normalized Wave Impedance in Positive Direction
$z^-$	Normalized Wave Impedance in Negative Direction
$\epsilon$	Permittivity
$\epsilon_0$	Permittivity in Free Space
$\mu$	Permeability

$\mu_0$	Permeability in Free Space
$\omega$	Angular Frequency
$\lambda$	Wavelength
$T$	Propagation Factor
$M$	Transfer Matrix
$m$	Elements of Transfer Matrix
$\Gamma$	Reflection Coefficient
$\xi$	Coupling Coefficient
$P$	Normalized Power
$\gamma$	Magneto-electric Damping Frequency
$L$	Length
$\Lambda$	Arbitrary parameter
$\Omega$	Arbitrary parameter
$d$	Thickness
$MM$	Metamaterial
$SRR$	Split Ring Resonator
$CST$	Computer Simulation Technology

## CHAPTER 1

### INTRODUCTION

#### 1.1 Background

We first present how the metamaterial concept emerged, and then give a brief literature review of isotropic and bi-anisotropic metamaterial. Finally, we discuss the motivation of the thesis. Just after World War II, metamaterials were developed and history of metamaterials shares a common history with artificial dielectrics in microwave engineering. However, at the end of the 19<sup>th</sup> century there are determining explorations of artificial materials for manipulating electromagnetic waves.

In the late 1940s, Dr. Winston E. Kock is the first researcher obtaining the materials having similar characteristics to metamaterials. Later Dr. Victor Veselago described theoretically materials possessing reversed physical characteristics to be discussed later on. Approximately 30 years later, in the year 2000, the experimental demonstration of functioning electromagnetic metamaterials was reported by Smith et al. with horizontally stacking, periodically, split-ring resonators and thin wire structures. Utilization of artificial lumped-element loaded transmission lines in microstrip technology method was provided in 2002 to realize negative index metamaterials. The first real invisibility cloak was realized in 2006, at microwave frequencies [1-6].

Several goals must be achieved for metamaterial applications to be realized, researcher in [7] stated that this suggestion. For finding ways to mass-produce the metamaterials, reducing energy loss, which is a major limiting factor, keep developing three-dimensional isotropic materials instead of planar structures [7].



All materials are made of atoms, which are dipoles so that it can also be applied to the this science. The light velocity of these dipoles is modified by a factor  $n$  (the refractive index). The role of atomic dipoles is done by the ring and wire: the wire acts as a ferroelectric atom, while the property of inductor is done by ring and the open section as a capacitor.

It is demonstrated that metallic wires aligned along the direction of propagation could provide a metamaterial with negative permittivity ( $\epsilon < 0$ ) [6]. The challenge was to construct a material which can also showed negative permeability ( $\mu < 0$ ) because natural materials (such as ferroelectrics) were already known to exist with negative permittivity.

The idea that a split ring (C shape) with its axis placed along the direction of wave propagation could provide a negative permeability was demonstrated in 1999 by Pendry [7].

## **1.2 Literature Review**

This subsection is divided into two reviews. We first deal with isotropic metamaterial, and then bi-anisotropic metamaterial.

### **1.2.1 Isotropic Metamaterial**

Metamaterials earn their properties not from their composition, but from their engineered structures. Creating material properties which are unachievable with conventional materials can be obtained by the precise shape, geometry, size, orientation and arrangement [8-10].

Investigation of materials with a negative refractive index is the primary research in metamaterials [3, 11-12]. The creation of super lenses can be realized by the negative refractive index materials having a spatial resolution below that of the wavelength. In addition to the electromagnetic metamaterials acoustic and seismic metamaterials are also areas of active research [13,14].

Many different applications of metamaterials are possible such as, sensor detection and infrastructure monitoring, smart solar power management, public safety, high-

frequency battlefield communication and lenses for high-gain antennas, improving ultrasonic sensors, and even shielding structures from earthquakes [14-18]. Physics and electromagnetism (especially optics and photonics) have become a new sub-discipline within metamaterials [19-21].

The huge potential of metamaterials is the possibility to create a structure with a negative refractive index, since nearly all materials encountered in optics (such as glass or water) have positive values for both permittivity  $\epsilon$  and permeability  $\mu$ .

Anisotropic starting materials with only negative permittivity can produce negative refraction due to chirality, although a material having either (but not both)  $\epsilon$  or  $\mu$  negative often does not transmit electromagnetic radiation.

Negative  $\epsilon$  and negative  $\mu$  can be realized by engineering metamaterials, meaning that negative refractive index for a material is possible. The real parts of both  $\epsilon_r$  and  $\mu_r$  do not have to be negative for a passive material to display negative refraction [22-24].

### **1.2.2 Bi-anisotropic metamaterials**

In many examples of electromagnetic metamaterials, the electric field causes magnetic polarization, and the magnetic field induces an electrical polarization, i.e., they affect each other proportionally (magneto-electric coupling). Such media are called as being bi-isotropic. Media which shows magneto-electric coupling, and which are also anisotropic, are referred to as bi-anisotropic [25, 27].

Related to magneto-electric coupling of bi-isotropic media, there are four material parameters are  $\epsilon$ ,  $\mu$ ,  $\kappa$  and  $\chi$ . Here  $\kappa$  and  $\chi$  means the strength of chirality and the Tellegen parameter respectively.

For an bi-isotropic media having different  $\kappa$  and  $\chi$  values, it is possible to obtain a backward wave and a forward wave can occur. Alternatively, two forward waves or two backward waves can also occur, depending on the strength of the chirality parameter.

It is well-known that metamaterials fabricated by an engineering design possess electromagnetic properties unavailable in conventional materials such as negative refractive index and perfect lens. Within the broad scope of metamaterials, bi-anisotropic metamaterials have properties different than isotropic metamaterials in that they have different forward and backward wave impedances, different forward and backward reflection scattering parameters, a wider stop-band compared to isotropic metamaterials, and a magneto-electric coupling coefficient [28-30]. Therefore, it is possible to realize different electromagnetic properties of materials comparing of bi-anisotropic metamaterials.

### **1.3 Motivation of the Thesis**

In the literature, wave propagation characteristics of different composite metamaterial media are investigated. To our best knowledge, wave propagation characteristics of a composite structure comprising of a bi-anisotropic metamaterial slab and an isotropic conventional slab has not yet been analyzed. In this thesis, our purpose is to investigate these characteristics of the aforementioned structure.

To achieve our goal, we first define the electromagnetic properties (wave impedances and propagation constants) of a bi-anisotropic metamaterial slab and a conventional material slab, and then derive forward and backward scattering parameters of the composite medium constructed by a cascade connection of these materials. Next, we analyze propagation characteristics of this composite structure using a commercial electromagnetic software program (CST Microwave Studio). Finally, we compare the simulated and numerically obtained results of wave propagation characteristics.

The aim of Chapter 2 is analytically present forward and backward transmission and reflection scattering parameters, as well as complex power relations of the composite structure constructed by a cascade connection of these materials.

The major point of Chapter 3 is to compare our derived equations with validation on Matlab. Then in chapter 4, we obtain forward and backward scattering parameters of a composite structure with a bianisotropic metamaterial and a conventional material by using commercial software program CST Microwave Studio.

In the last chapter, a brief summary and discussion of the results obtained during this thesis work are included. Additionally, future works and further studies for potential applications of the composite bi-anisotropic metamaterials are also suggested in the same chapter.

## CHAPTER 2

### THEORETICAL ANALYSIS OF PROPAGATION CHARACTERISTICS OF A COMPOSITE STRUCTURE CONSISTING OF A BI-ANISOTROPIC METAMATERIAL AND A CONVENTIONAL MATERIAL

#### 2.1 Introduction

In this chapter, our aim is to analyze propagation characteristics of a composite structure composed of a bi-anisotropic metamaterial slab and a conventional material as shown in Figure 2.1. Toward this end, we first derive forward and backward reflection and transmission scattering (S-) parameters and then analyze forward and backward reflected, transmitted, and loss powers of this composite structure. This chapter is organized as follows. In Section 2.2, we first present general field and impedance expressions of a bi-anisotropic metamaterial to put the subsequent derivations into right perspective and to demonstrate the wave characteristics of a bianisotropic metamaterial slab. Next, in Section 2.3, we derive forward and backward reflection and transmission S-parameters of the composite structure by considering two different reference configurations. Finally, in Section 2.4, we give the derived forward and backward reflected, transmitted, and loss powers using these reference configurations.

Throughout the theoretical analysis in this Chapter, we assume that bi-anisotropic metamaterial slab and conventional material (Figure 2.1) both extend to infinity in  $y$ - and  $z$ -directions. We also assume that a uniform plane wave is normal incident to the composite structure and that time reference in the form  $\exp(-i\omega t)$  is utilized in all derivations.

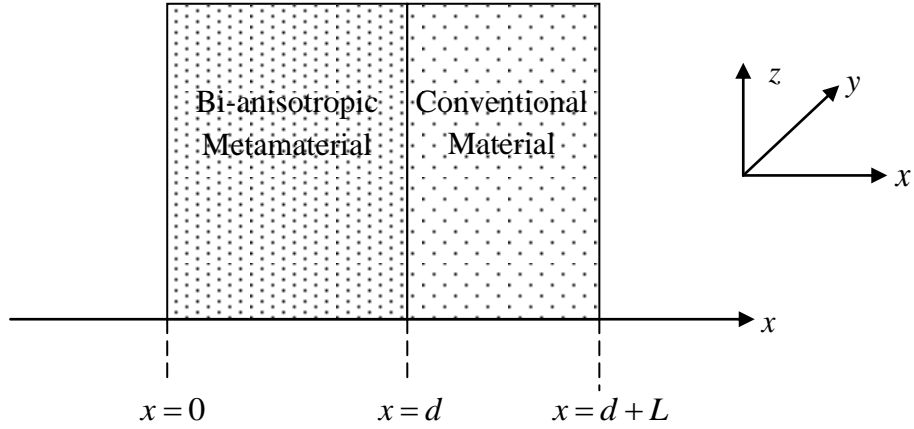


**Figure 2.1:** Composite structure composed of bi-anisotropic and isotropic slab ( The problem under investigation ).

## 2.2 General Field Expressions of a Bi-anisotropic Metamaterial Slab

To understand the behavior of forward and backward reflection and transmission S-parameters as well as power and propagation characteristics, in this chapter we give general field and impedance expressions in a bi-anisotropic metamaterial slab. For the assumed time reference, Maxwell's equations read as

$$\vec{\nabla} \times \vec{E}(\vec{r}) = i\omega \vec{B}(\vec{r}), \quad (2.1)$$

$$\vec{\nabla} \times \vec{H}(\vec{r}) = -i\omega \vec{D}(\vec{r}), \quad (2.2)$$

$$\vec{\nabla} \cdot \vec{D} = \rho_{ev} = 0, \quad (2.3)$$

$$\vec{\nabla} \cdot \vec{B} = 0, \quad (2.4)$$

where it has been assumed that there is no-free charge density inside the slab.

To describe the macroscopic behavior of the slab, the following constitutive relations can be utilized [29],

$$\vec{D} = \overset{=}{\varepsilon} \cdot \vec{E} + \overset{=}{\xi} \cdot \vec{H}, \quad (2.5)$$

$$\vec{B} = \vec{\mu} \cdot \vec{H} + \vec{\zeta} \cdot \vec{E}, \quad (2.6)$$

where

$$\vec{\varepsilon} = \varepsilon_0 \begin{pmatrix} \varepsilon_{xx} & 0 & 0 \\ 0 & \varepsilon_{yy} & 0 \\ 0 & 0 & \varepsilon_{zz} \end{pmatrix}, \quad \vec{\mu} = \mu_0 \begin{pmatrix} \mu_{xx} & 0 & 0 \\ 0 & \mu_{yy} & 0 \\ 0 & 0 & \mu_{zz} \end{pmatrix}, \quad (2.7)$$

$$\vec{\xi} = \frac{1}{c} \begin{pmatrix} 0 & 0 & 0 \\ 0 & 0 & 0 \\ 0 & -i\xi_0 & 0 \end{pmatrix}, \quad \vec{\zeta} = \frac{1}{c} \begin{pmatrix} 0 & 0 & 0 \\ 0 & 0 & i\xi_0 \\ 0 & 0 & 0 \end{pmatrix}. \quad (2.8)$$

In (2.7) and (2.8),  $\varepsilon_{xx}$  ( $\mu_{xx}$ ),  $\varepsilon_{yy}$  ( $\mu_{yy}$ ), and  $\varepsilon_{zz}$  ( $\mu_{zz}$ ) are the relative complex permittivities (permeabilities) in  $x$ -,  $y$ -, and  $z$ -directions, respectively;  $\varepsilon_0$ ,  $\mu_0$ , and  $c$  are, respectively, the permittivity and permeability of free-space and the phase velocity of light in free-space; and  $\xi_0$  is the magneto-electric coupling coefficient.

Substitution of (2.7) and (2.8) into (2.5) and (2.6), we obtain

$$\begin{bmatrix} D_x \\ D_y \\ D_z \end{bmatrix} = \varepsilon_0 \begin{bmatrix} \varepsilon_{xx} E_x \\ \varepsilon_{yy} E_y \\ \varepsilon_{zz} E_z - i\xi_0 H_y / (\varepsilon_0 c) \end{bmatrix}, \quad (2.9)$$

$$\begin{bmatrix} B_x \\ B_y \\ B_z \end{bmatrix} = \mu_0 \begin{bmatrix} \mu_{xx} H_x \\ \mu_{yy} H_y + \frac{i\xi_0}{\mu_0 c} E_z \\ \mu_{zz} H_z \end{bmatrix}. \quad (2.10)$$

Using (2.9) and (2.10) and after some manipulations, the following relations can be found

$$\frac{\partial E_z}{\partial y} - \frac{\partial E_y}{\partial z} = i\omega B_x = i\omega\mu_0\mu_{xx}H_x, \quad (2.11)$$

$$\frac{\partial H_y}{\partial x} - \frac{\partial H_x}{\partial y} = -i\omega D_z, \quad \left[ \frac{\omega\xi_0}{c} + \frac{\partial}{\partial x} \right] H_y - \frac{\partial H_x}{\partial y} = -i\omega\varepsilon_0\varepsilon_{zz}E_z. \quad (2.12)$$

In our theoretical analysis, we assume that a uniform plane wave with a linear polarization in  $z$ -direction impinges onto the slab. Because, electric field in free-space,  $\vec{E}_0$ , has only a tangential component and no axial (longitudinal) component, according to the boundary conditions (continuity of tangential (normal) component of  $\vec{E}$  ( $\vec{D}$ ) over the free-space-metamaterial slab interface must be continuous), no axial component of electric field inside the metamaterial slab,  $\vec{E}_s$ , results in

$$\hat{a}_z \cdot (\vec{D}_s - \vec{D}_0) = 0, \quad D_{sn} = D_{0n}, \quad D_{sn} = \epsilon_0 \epsilon_{xx} E_{sx} = 0 \quad \Rightarrow \quad E_{sx} = 0. \quad (2.13)$$

Here,  $E_{sx}$  is the component of electric field of the slab in  $x$ -direction.

In addition, according to the continuity of tangential component over the boundary, vanishing of  $\vec{E}_0$  in  $y$ -direction in free-space forces vanishing of  $\vec{E}_s$  in  $y$ -direction in the slab; that is  $E_{sy} = 0$ .

Despite the fact that in free-space wave propagates only in  $x$ -direction, we have  $\partial/\partial y = \partial/\partial z = 0$  due to the fact that the slab extends to infinity in  $y$ - and  $z$ -directions. Reflecting this condition into (2.11) and (2.12), we find

$$i\omega\mu_0\mu_{xx}H_{sx} = 0, \quad H_{sx} = 0, \quad (2.14)$$

$$\left[ \frac{\omega\xi_0}{c} + \frac{\partial}{\partial x} \right] H_{sy} = -i\omega\epsilon_0\epsilon_{zz}E_{sz}. \quad (2.15)$$

Besides, incorporating  $E_{sx} = 0$  and  $E_{sy} = 0$  into (2.14) and (2.15), we determine

$$\frac{\partial H_{sz}}{\partial x} = 0, \quad H_{sz} = 0, \quad (2.16)$$

$$\left[ \frac{\omega\xi_0}{c} + \frac{\partial}{\partial x} \right] H_{sy} = -i\omega\epsilon_0\epsilon_{zz}E_{sz}. \quad (2.17)$$



Because  $E_{sz}$  does not vanish inside the slab, we could determine a dispersion relation based on this term as follows. From (2.17) and (2.16)

$$\left[ \frac{\partial^2}{\partial x^2} + k_x^2 \right] = 0. \quad k_x = k_0 n, \quad n = \sqrt{\varepsilon_{zz} \mu_{yy} - \xi_0^2}, \quad (2.18)$$

where  $k_x$  is the propagation constant of the bianisotropic metamaterial slab (in  $x$ -direction).

The solution of (2.18) is in the form

$$\left( D^2 + k_x^2 \right) E_{sz} = 0, \quad E_{sz} = E_{sz}^+ e^{ik_x x} + E_{sz}^- e^{-ik_x x}. \quad (2.19)$$

In a similar fashion, from (2.16) and (2.17), we get

$$\frac{1}{-i\omega\varepsilon_0\varepsilon_{zz}} \left[ \frac{\omega\xi_0}{c} - \frac{\partial}{\partial x} \right] \left[ \frac{\omega\xi_0}{c} + \frac{\partial}{\partial x} \right] H_{sy} = i\omega\mu_0\mu_{yy}H_{sy}, \quad (2.20)$$

$$\left[ \left( \frac{\omega\xi_0}{c} \right)^2 - \frac{\partial^2}{\partial x^2} \right] H_{sy} = k_0^2 \mu_{yy} \varepsilon_{zz} H_{sy}, \quad (2.21)$$

$$H_{sy} = H_{sy}^+ e^{ik_x x} + H_{sy}^- e^{-ik_x x}. \quad (2.22)$$

In addition to expressions of electric and magnetic fields, it is also instructive to present the expressions of forward and backward wave impedances to understand the propagation characteristics of the composite structure in Figure 2.1. To achieve that goal, substituting (2.19) and (2.22) into (2.16) and assuming only the wave travelling in  $+x$  direction exists, we find

$$\left(\frac{\omega\xi_0}{c} - ik_x\right) E_{sz}^+ e^{ik_x x} = i\omega\mu_0\mu_{yy} H_{sy}^+ e^{ik_x x}, \quad (2.23)$$

$$k_0(\xi_0 - in) E_{sz}^+ = i\omega\mu_0\mu_{yy} H_{sy}^+. \quad (2.24)$$

From (2.24) and (2.18), we obtain the expression of wave impedance in  $x$ -direction (forward) as

$$Z_x^+ = Z_{\text{TE}_2} = \frac{E_{sz}^+}{-H_{sy}^+} = \frac{\omega\mu_0\mu_{yy}}{k_0(n + i\xi_0)} = Z_0 \frac{\mu_{yy}}{(n + i\xi_0)}, \quad Z_0 = \sqrt{\frac{\mu_0}{\varepsilon_0}}. \quad (2.25)$$

Furthermore, substituting (2.19) and (2.22) into (2.17) and assuming only the wave travelling in  $+x$ -direction exists, we find

$$\left(\frac{\omega\xi_0}{c} + ik_x\right) H_{sy}^+ e^{ik_x x} = -i\omega\varepsilon_0\varepsilon_{zz} E_{sz}^+ e^{ik_x x}, \quad (2.26)$$

$$-k_0(n - i\xi_0) H_{sy}^+ = \omega\varepsilon_0\varepsilon_{zz} E_{sz}^+. \quad (2.27)$$

From (2.27) and (2.18), we obtain

$$Z_x^+ = Z_{\text{TE}_2} = \frac{E_{sz}^+}{-H_{sy}^+} = \frac{k_0(n - i\xi_0)}{\omega\varepsilon_0\varepsilon_{zz}} = Z_0 \frac{(n - i\xi_0)}{\varepsilon_{zz}}, \quad Z_0 = \sqrt{\frac{\mu_0}{\varepsilon_0}}. \quad (2.28)$$

Therefore, from (2.25) and (2.28), we find

$$\frac{\mu_{yy}}{(n + i\xi_0)} = \frac{(n - i\xi_0)}{\varepsilon_{zz}}, \quad \varepsilon_{zz}\mu_{yy} = n^2 + \xi_0^2, \quad (2.29)$$

which validates (2.18).

On the other hand, for waves travelling in  $-x$ -direction, from (2.16) and (2.17), we find the expression of wave impedance in  $-x$ -direction (backward) as

$$Z_x^- = -\frac{E_{sz}^-}{-H_{sy}^-} = \frac{\omega\mu_0\mu_{yy}}{(k_x - ik_0\xi_0)} = Z_0 \frac{\mu_{yy}}{(n - i\xi_0)}, \quad \frac{k_x}{k_0} = n, \quad (2.30)$$

$$Z_x^- = -\frac{E_{sz}^-}{-H_{sy}^-} = \frac{k_0(n + i\xi_0)}{\omega\varepsilon_0\varepsilon_{zz}} = Z_0 \frac{(n + i\xi_0)}{\varepsilon_{zz}}. \quad (2.31)$$

It is seen that the wave impedances in the slab in  $-x$ -direction in (2.30) and (2.31) are equal.

As a result, for waves travelling positive and negative  $x$  directions, their respective normalized wave impedances with respect to air are

$$z_x^+ = \frac{\mu_{yy}}{n + i\xi_0}, \quad z_x^- = \frac{\mu_{yy}}{n - i\xi_0}. \quad (2.32)$$

## 2.3 Forward and Backward Reflection and Transmission Scattering Parameters

In this chapter, our aim is to derive forward and backward reflection and transmission S-parameters since these parameters are utilized to analyze the propagation characteristics of the composite structure in Figure 2.1. Because, as shown in (2.32), the bi-anisotropic metamaterial slab possesses two different normalized forward and backward wave impedances, it demonstrates a reflection asymmetric property ( $S_{11} \neq S_{22}$  where  $S_{11}$  and  $S_{22}$  denote, respectively, the forward and backward reflection S-parameters) [30]. Whereas reflection properties present an insight into the reflection characteristics, transmission properties demonstrate propagation characteristics. Therefore, since reflection and transmission properties are independent properties for electromagnetic characterization of materials, for a comprehensive and concrete analysis, these two properties must simultaneously be analyzed.

To better present the derivations in this chapter, we present the derivations in two sections. In the first section, we concentrate on obtaining forward reflection and transmission S-parameters of the composite structure in Figure 2.1 while in second section we focus on determining backward reflection and transmission S-parameters of the same structure.

### 2.3.1 Forward Reflection and Transmission Scattering Parameters

In the derivations of forward reflection and transmission S-parameters of the structure in Figure 2.1, we analyze the problem shown in Figure 2.2. Considering this problem, we can write the following expressions for electric and magnetic fields for each medium (here it is assumed that first and fourth media are air).

For 1<sup>st</sup> medium,

$$\vec{E}_I = \hat{a}_z \left( E_I^+ e^{ik_0x} + E_I^- e^{-ik_0x} \right), \quad (2.33)$$

$$\vec{H}_I = \hat{a}_y \frac{1}{Z_0} \left( -E_I^+ e^{ik_0x} + E_I^- e^{-ik_0x} \right). \quad (2.34)$$

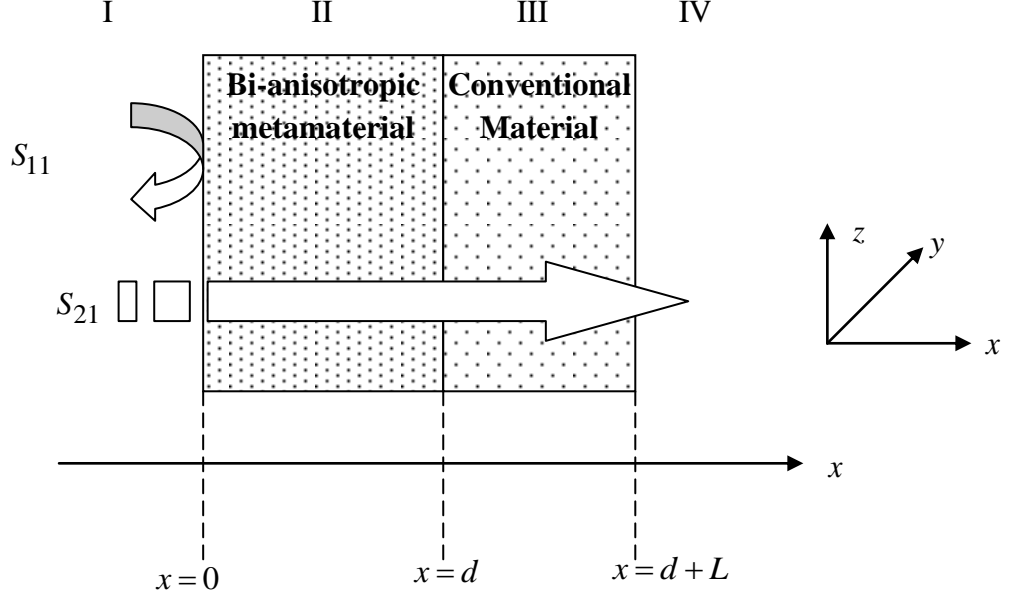


**Figure 2.2:** Analysis of composite structure in a forward direction.

For 2<sup>nd</sup> medium,

$$\vec{E}_{II} = \hat{a}_z \left( E_{II}^+ e^{ik_x x} + E_{II}^- e^{-ik_x x} \right), \quad (2.35)$$

$$\vec{H}_{II} = \hat{a}_y \left( -\frac{E_{II}^+}{Z^+} e^{ik_x x} + \frac{E_{II}^-}{Z^-} e^{-ik_x x} \right). \quad (2.36)$$

For 3<sup>rd</sup> medium,

$$\vec{E}_{III} = \hat{a}_z \left( E_{III}^+ e^{ik_{01} x} + E_{III}^- e^{-ik_{01} x} \right), \quad (2.37)$$

$$\vec{H}_{III} = \hat{a}_y \frac{1}{Z_1} \left( -E_{III}^+ e^{ik_{01} x} + E_{III}^- e^{-ik_{01} x} \right). \quad (2.38)$$

For 4<sup>th</sup> medium,

$$\vec{E}_{IV} = \hat{a}_z E_{IV}^+ e^{ik_0 x}, \quad (2.39)$$

$$\vec{H}_{IV} = -\hat{a}_y \frac{1}{Z_0} E_{IV}^+ e^{ik_0 x}. \quad (2.40)$$

In (2.33)-(2.40),  $Z_0$ ,  $Z_1$ ,  $Z^+$ , and  $Z^-$  are, respectively, the impedances of free-space, the conventional material, and the bi-anisotropic metamaterial slab (forward and backward);  $k_0$ ,  $k_{01}$ , and  $k_x$  are propagation constants (wavenumbers) of free-space, the conventional material, and the bianisotropic metamaterial slab. In the analysis, it is presumed that while there is only one travelling wave in fourth medium (air), there are two waves travelling in opposite direction for other media in Figure 2.2.

Explicit expressions of propagation constants and wave impedances of the conventional material and the slab are

$$k_0 = \omega\sqrt{\varepsilon_0\mu_0}, \quad k_{01} = k_0\sqrt{\varepsilon_r\mu_r}, \quad (2.41)$$

$$Z_0 = \sqrt{\frac{\mu_0}{\varepsilon_0}}, \quad Z_1 = Z_0\sqrt{\frac{\mu_r}{\varepsilon_r}}, \quad (2.42)$$

where  $\varepsilon_r$  and  $\mu_r$  are, respectively, the relative complex permittivity and relative complex permeability of the conventional material. The explicit expressions of propagation constants and (normalized) wave impedances of the slab can be found in (2.18) and (2.32).

Boundary conditions are the conditions that fields of electromagnetic waves must satisfy only over the boundary. Enforcing the necessary and corresponding boundary conditions at boundaries  $x=0$ ,  $x=d$ , and  $x=d+L$  allows us to determine the forward reflection and transmission S-parameters (in addition to the field coefficient in (2.33)-(2.40) if the strength of the source is given/known).

### 2.3.1.1 Derivation of Forward Reflection Scattering Parameter

In the derivation of reflection S-parameters, the general procedure is to first apply the boundary conditions at the boundary far distant from the source, and then propagate toward the boundary at the source region [31]. Using this procedure, we first apply the boundary conditions at  $x=d+L$  and find a relation between  $E_{III}^+$  and  $E_{III}^-$  as

$$E_{III}^+ = \Lambda_1 E_{III}^-, \quad \Lambda_1 = \frac{Z_0 + Z_1}{Z_0 - Z_1} e^{-2ik_{01}(d+L)}. \quad (2.43)$$

Incorporating (2.43) with (2.37) and (2.38), we obtain

$$\vec{E}_{III} = \hat{a}_z E_{III}^- \left( \Lambda_1 e^{ik_{01}x} + e^{-ik_{01}x} \right), \quad \vec{H}_{III} = \hat{a}_y \frac{E_{III}^-}{Z_1} \left( -\Lambda_1 e^{ik_{01}x} + e^{-ik_{01}x} \right). \quad (2.44)$$

Then, applying the boundary conditions at  $x=d$  and using (2.35), (2.36), and (2.44), we determine (dividing the boundary conditions obtained from the continuity of tangential components of electric and magnetic fields at the interface  $x=d$  in order to eliminate the unknown  $E_{III}^-$ )

$$\frac{E_{II}^+ e^{ik_x d} + E_{II}^- e^{-ik_x d}}{-\frac{E_{II}^+}{Z^+} e^{ik_x d} + \frac{E_{II}^-}{Z^-} e^{-ik_x d}} = \frac{E_{III}^- \left( \Lambda_1 e^{ik_{01}d} + e^{-ik_{01}d} \right)}{\frac{E_{III}^-}{Z_1} \left( -\Lambda_1 e^{ik_{01}d} + e^{-ik_{01}d} \right)} = \frac{Z_1 \left( \Lambda_1 e^{ik_{01}d} + e^{-ik_{01}d} \right)}{-\Lambda_1 e^{ik_{01}d} + e^{-ik_{01}d}}. \quad (2.45)$$

$$E_{II}^- = \Lambda_3 E_{II}^+, \quad (2.46)$$

where

$$\Lambda_3 = \frac{\left(\frac{\Lambda_2}{Z^+} - 1\right)}{\left(\frac{\Lambda_2}{Z^-} + 1\right)} e^{i2k_x d}, \quad \Lambda_2 = \frac{Z_1 \left(\Lambda_1 e^{ik_{01}d} + e^{-ik_{01}d}\right)}{\Lambda_1 e^{ik_{01}d} - e^{-ik_{01}d}}. \quad (2.47)$$

We follow the procedure by substituting the relation between  $E_{II}^+$  and  $E_{II}^-$  in (2.46) into (2.35) and (2.36) and determine

$$\vec{E}_{II} = \hat{a}_z E_{II}^+ \left( e^{ik_x x} + \Lambda_3 e^{-ik_x x} \right), \quad \vec{H}_{II} = \hat{a}_y E_{II}^+ \left( -\frac{1}{Z^+} e^{ik_x x} + \frac{\Lambda_3}{Z^-} e^{-ik_x x} \right). \quad (2.48)$$

Finally, applying the boundary condition (continuity of the tangential components of electric and magnetic fields in each respective region) at  $x=0$  and using (2.33), (2.34) and (2.48), we obtain the forward reflection S-parameter ( $S_{11}$ )

$$\frac{E_I^+ + E_I^-}{\frac{1}{Z_0} (-E_I^+ + E_I^-)} = \frac{E_{II}^+ (1 + \Lambda_3)}{E_{II}^+ \left( -\frac{1}{Z^+} + \frac{\Lambda_3}{Z^-} \right)} = \frac{1 + \Lambda_3}{-\frac{1}{Z^+} + \frac{\Lambda_3}{Z^-}}, \quad (2.49)$$

$$\frac{E_I^+ + E_I^-}{E_I^+ - E_I^-} = \frac{1 + \Lambda_3}{\frac{Z_0}{Z^+} - \frac{Z_0 \Lambda_3}{Z^-}} = \Lambda_4, \quad (2.50)$$

$$r = S_{11} = \frac{E_I^-}{E_I^+} e^{+2ik_0(d+L)} = \frac{(\Lambda_4 - 1)}{(\Lambda_4 + 1)}. \quad (2.51)$$



### 2.3.1.2 Derivation of Forward Transmission Scattering Parameter

Different from the derivation of reflection S-parameter in the previous subsection, in the derivation of the forward transmission S-parameter, we apply the necessary and corresponding boundary conditions in a manner of forward-direction (or in the direction of wave travel) [31]. It is also possible to utilize backward-direction concept in the derivation of forward transmission S-parameter. In this subsection, we derive the transmission S-parameter using backward-direction concept (although the derived expression of transmission S-parameters is the same for forward and backward directions).

Toward this end, we first apply the boundary conditions at  $x = d + L$

$$E_{III}^+ e^{ik_{01}(d+L)} + E_{III}^- e^{-ik_{01}(d+L)} = E_{IV}^+ e^{ik_0(d+L)}, \quad (2.52)$$

$$\frac{1}{Z_1} \left( -E_{III}^+ e^{ik_{01}(d+L)} + E_{III}^- e^{-ik_{01}(d+L)} \right) = -\frac{1}{Z_0} E_{IV}^+ e^{ik_0(d+L)}. \quad (2.53)$$

Then, from (2.52) and (2.53) we determine a relation between  $E_{III}^-$  and  $E_{IV}^+$  as

$$E_{III}^+ = E_{IV}^+ \Omega_1, \quad \Omega_1 = \frac{1}{2} \left( 1 + \frac{Z_1}{Z_0} \right) e^{ik_0(d+L)} e^{-ik_{01}(d+L)}, \quad (2.54)$$

$$E_{IV}^+ = \Omega_2 E_{III}^-, \quad \Omega_2 = \frac{e^{-ik_{01}(d+L)}}{\Omega_1 e^{ik_{01}(d+L)} - \frac{Z_1}{Z_0} e^{ik_0(d+L)}}, \quad (2.55)$$

$$E_{III}^- = E_{IV}^+ \Omega_2, \quad \Omega_2 = \left[ -\frac{Z_1}{Z_0} e^{ik_0(d+L)} + \Omega_1 e^{ik_{01}(d+L)} \right] e^{+ik_{01}(d+L)}. \quad (2.56)$$

In (2.56) eliminating  $\Omega_1$  from this equation and letting  $\Omega_2$  alone, we get

$$E_{III}^- = E_{IV}^+ \Omega_2, \quad \Omega_2 = \frac{1}{2} \left( 1 - \frac{Z_1}{Z_0} \right) e^{ik_0(d+L)} e^{+ik_{01}(d+L)}. \quad (2.57)$$

Incorporating (2.56) and (2.57) with (2.37) and (2.38), we obtain

$$\bar{E}_{III} = \hat{a}_z E_{IV}^+ \left( \Omega_1 e^{ik_{01}x} + \Omega_2 e^{-ik_{01}x} \right), \quad (2.58)$$

$$\bar{H}_{III} = \hat{a}_y \frac{1}{Z_1} E_{IV}^+ \left( -\Omega_1 e^{ik_{01}x} + \Omega_2 e^{-ik_{01}x} \right), \quad (2.59)$$

We follow the backward direction concept and applying boundary conditions at  $x = d$ , yielding

$$E_{II}^+ e^{ik_x d} + E_{II}^- e^{-ik_x d} = E_{IV}^+ \left( \Omega_1 e^{ik_{01}d} + \Omega_2 e^{-ik_{01}d} \right), \quad (2.60)$$

$$-\frac{E_{II}^+}{Z^+} e^{ik_x d} + \frac{E_{II}^-}{Z^-} e^{-ik_x d} = \frac{1}{Z_1} E_{IV}^+ \left( -\Omega_1 e^{ik_{01}d} + \Omega_2 e^{-ik_{01}d} \right). \quad (2.61)$$

Incorporating (2.60) and (2.61) together, we obtain another single constant  $\Omega_3$  as

$$E_{II}^+ = E_{IV}^+ \Omega_3, \quad (2.62)$$

where

$$\Omega_3 = \frac{1}{\left( 1 + \frac{Z^-}{Z^+} \right)} \left[ \Omega_1 \left( 1 + \frac{Z^-}{Z_1} \right) e^{ik_{01}d} + \Omega_2 \left( 1 - \frac{Z^-}{Z_1} \right) e^{-ik_{01}d} \right] e^{-ik_x d}. \quad (2.63)$$

Writing all parameters in a single  $\Omega_4$  parameter makes our equation easier,

$$E_{II}^- = E_{IV}^+ \Omega_4, \quad \Omega_4 = \left( \Omega_1 e^{ik_0 d} + \Omega_2 e^{-ik_0 d} - \Omega_3 e^{+ik_x d} \right) e^{+ik_x d}. \quad (2.64)$$

Finally applying the boundary conditions at  $x=0$ , we obtain

$$E_I^+ + E_I^- = E_{II}^+ + E_{II}^-, \quad (2.65)$$

$$\frac{1}{Z_0} \left( -E_I^+ + E_I^- \right) = -\frac{E_{II}^+}{Z^+} + \frac{E_{II}^-}{Z^-}. \quad (2.66)$$

Eliminating  $E_I^-$  from (2.65) and (2.66), we determine

$$E_I^+ = \frac{1}{2} \left\{ E_{II}^+ \left( 1 + \frac{Z_0}{Z^+} \right) + E_{II}^- \left( 1 - \frac{Z_0}{Z^-} \right) \right\}. \quad (2.67)$$

Incorporating (2.62) and (2.64) into (2.67), we derive

$$E_I^+ = E_{IV}^+ \frac{1}{2} \left\{ \Omega_3 \left( 1 + \frac{Z_0}{Z^+} \right) + \Omega_4 \left( 1 - \frac{Z_0}{Z^-} \right) \right\}, \quad (2.68)$$

$$S_{21} = \frac{E_{IV}^+}{E_I^+} e^{+2ik_0(d+L)} = \frac{2e^{+2ik_0(d+L)}}{\Omega_3 \left( 1 + \frac{Z_0}{Z^+} \right) + \Omega_4 \left( 1 - \frac{Z_0}{Z^-} \right)}. \quad (2.69)$$

### 2.3.2 Backward Reflection and Transmission Scattering Parameter

Here, in the derivations of backward reflection and transmission S-parameters of the structure in Figure 2.1, we analyze the problem shown in Figure 2.3. Considering this problem, we can write the following expressions for electric and magnetic fields for each medium (here it is assumed that first and fourth media are air)

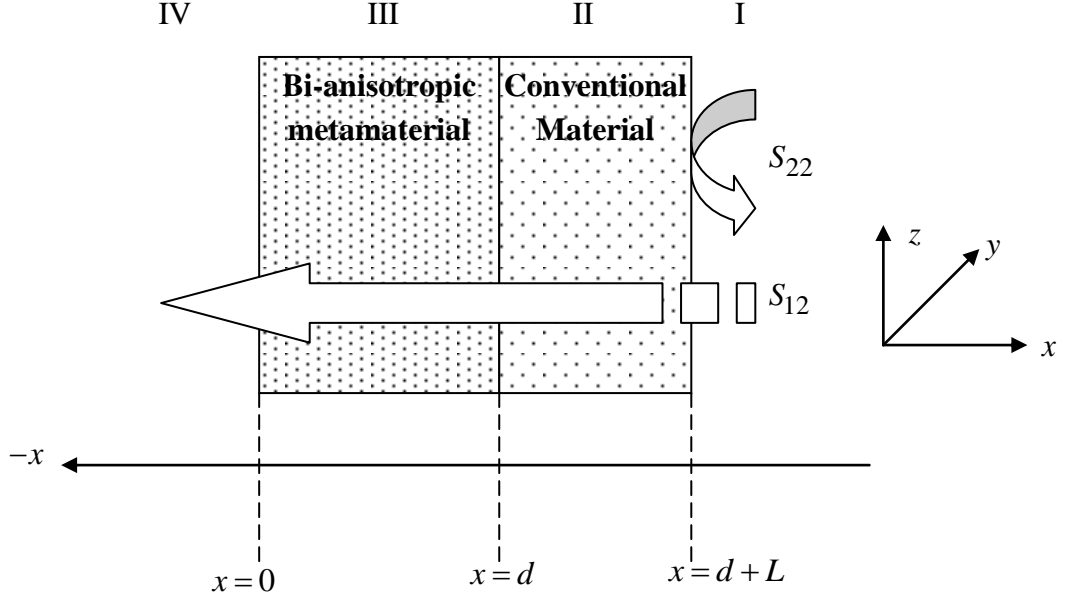


**Figure 2.3:** Analysis of composite structure in a backward direction.

For 1<sup>st</sup> medium,

$$\vec{E}_{Ib} = \hat{a}_z \left( E_{Ib}^+ e^{-ik_0x} + E_{Ib}^- e^{+ik_0x} \right), \quad (2.70)$$

$$\vec{H}_{Ib} = \hat{a}_y \frac{1}{Z_0} \left( E_{Ib}^+ e^{-ik_0x} - E_{Ib}^- e^{+ik_0x} \right). \quad (2.71)$$

For 2<sup>nd</sup> medium,

$$\vec{E}_{IIb} = \hat{a}_z \left( E_{IIb}^+ e^{-ik_{01}x} + E_{IIb}^- e^{+ik_{01}x} \right), \quad (2.72)$$

$$\vec{H}_{IIb} = \hat{a}_y \frac{1}{Z_1} \left( E_{IIb}^+ e^{-ik_{01}x} - E_{IIb}^- e^{+ik_{01}x} \right). \quad (2.73)$$

For 3<sup>rd</sup> medium,

$$\vec{E}_{IIIb} = \hat{a}_z \left( E_{IIIb}^+ e^{-ik_x x} + E_{IIIb}^- e^{+ik_x x} \right), \quad (2.74)$$

$$\vec{H}_{IIIb} = \hat{a}_y \left( \frac{E_{IIIb}^+}{Z^-} e^{-ik_x x} - \frac{E_{IIIb}^-}{Z^+} e^{+ik_x x} \right). \quad (2.75)$$

For 4<sup>th</sup> medium,

$$\vec{E}_{IVb} = \hat{a}_z E_{IVb}^+ e^{-ik_0 x}, \quad (2.76)$$

$$\vec{H}_{IVb} = \hat{a}_y \frac{1}{Z_0} E_{IVb}^+ e^{-ik_0 x}. \quad (2.77)$$

In (2.70)-(2.77),  $Z_0$ ,  $Z_1$ ,  $Z^+$ , and  $Z^-$  are, respectively, the impedances of free-space, the conventional material, and the bi-anisotropic metamaterial slab (forward and backward);  $k_0$ ,  $k_{01}$ , and  $k_x$  are propagation constants (wavenumbers) of free-space, the conventional material, and the bianisotropic metamaterial slab. In the analysis, it is presumed that while there is only one travelling wave in fourth medium (air), there are two waves travelling in opposite direction for other media in Figure 2.3.

Propagation constants, wave impedances and other parameters of the conventional material and the slab are taken the same with previous section. Boundary conditions are the conditions that fields of electromagnetic waves must satisfy only over the boundary. Enforcing the necessary and corresponding boundary conditions at boundaries  $x=0$ ,  $x=d$ , and  $x=d+L$  allows us to determine the backward reflection and transmission S-parameters (in addition to the field coefficient in (2.70)-(2.77) if the strength of the source is given/known).

### 2.3.2.1 Derivation of Backward Reflection Scattering Parameter

In the derivation of reflection S-parameters, the general procedure is to first apply the boundary conditions at the boundary far distant from the source, and then propagate

toward the boundary at the source region [31]. As you followed previous subsection the same procedures also can be applied in this subsection. Using this procedure, we first apply the boundary conditions at  $x = d + L$  and find a relation between  $E_{IIIb}^+$  and  $E_{IIIb}^-$  as

$$E_{IIIb}^- = \frac{\left(\frac{1}{z^-} - 1\right)}{\left(1 + \frac{1}{z^+}\right)} E_{IIIb}^+. \quad (2.78)$$

Then, applying the boundary conditions at  $x = d$  and using(2.72), (2.73), and (2.78), we determine (dividing the boundary conditions obtained from the continuity of tangential components of electric and magnetic fields at the interface  $x = d$  in order to eliminate the unknown  $E_{III}^-$  )

$$E_{IIb}^- = \frac{(\Lambda_9 - 1)}{(\Lambda_9 + 1)} E_{IIb}^+ e^{-2ik_0d}, \quad \Lambda_9 = \frac{\left(1 + \frac{1}{z^+}\right) e^{-ik_xd} + \left(\frac{1}{z^-} - 1\right) e^{+ik_xd}}{\frac{z_1}{z^-} \left(1 + \frac{1}{z^+}\right) e^{-ik_xd} - \frac{z_1}{z^+} \left(\frac{1}{z^-} - 1\right) e^{+ik_xd}}. \quad (2.79)$$

Finally, applying the boundary condition (continuity of the tangential components of electric and magnetic fields in each respective region) at  $x=0$  and using(2.70), (2.71) and (2.79), we obtain the backward reflection S-parameter ( $S_{22}$ )

$$\frac{E_{Ib}^+ e^{-ik_0(d+L)} + E_{Ib}^- e^{+ik_0(d+L)}}{E_{Ib}^+ e^{-ik_0(d+L)} - E_{Ib}^- e^{+ik_0(d+L)}} = \Lambda_{10}, \quad \Lambda_{10} = z_1 \frac{(\Lambda_9 + 1) + (\Lambda_9 - 1) e^{+2ik_0L}}{(\Lambda_9 + 1) - (\Lambda_9 - 1) e^{+2ik_0L}}, \quad (2.80)$$

$$\frac{E_{Ib}^-}{E_{Ib}^+} = \frac{(\Lambda_{10} - 1)}{(\Lambda_{10} + 1)} e^{-2ik_0(d+L)}, \quad S_{22} = \frac{E_{Ib}^- e^{+2ik_0(d+L)}}{E_I^+} = \frac{\Lambda_{10} - 1}{\Lambda_{10} + 1}. \quad (2.81)$$

### 2.3.2.2 Derivation of Backward Transmission Scattering Parameter

Different from the derivation of reflection S-parameter in the previous subsection, in the derivation of the backward transmission S-parameter, we apply the necessary and corresponding boundary conditions in a manner of forward-direction (or in the direction of wave travel) [31]. It is also possible to utilize backward-direction concept in the derivation of backward transmission S-parameter. In this subsection, we derive the transmission S-parameter using backward-direction concept (although the derived expression of transmission S-parameters is the same for forward and backward directions).

Toward this end, we first apply the boundary conditions at  $x=0$  for the Figure 2.3 we obtain from equation (2.76)-(2.77) and (2.74)-(2.75),

$$E_{IVb}^+ = E_{IIIb}^+ + E_{IIIb}^-, \quad (2.82)$$

$$E_{IVb}^+ = \frac{E_{IIIb}^+}{z^-} - \frac{E_{IIIb}^-}{z^+}. \quad (2.83)$$

Getting  $E_{IIIb}^+$  and  $E_{IIIb}^-$  dependent with  $E_{IVb}^+$  in a different equation,

$$E_{IIIb}^+ = \frac{z^- (1+z^+)}{(z^+ + z^-)} E_{IVb}^+, \quad E_{IIIb}^- = \frac{z^+ (1-z^-)}{(z^+ + z^-)} E_{IVb}^+. \quad (2.84)$$

Now, we can write third medium equations with respect to  $E_{IVb}^+$  as,

$$\vec{E}_{IIIb} = \hat{a}_z \left( \frac{z^- (1+z^+)}{(z^+ + z^-)} e^{-ik_x x} + \frac{z^+ (1-z^-)}{(z^+ + z^-)} e^{+ik_x x} \right) E_{IVb}^+, \quad (2.85)$$

$$\vec{H}_{IIIb} = \hat{a}_y \left( \frac{1}{Z^-} \frac{z^- (1+z^+)}{(z^+ + z^-)} e^{-ik_x x} - \frac{1}{Z^+} \frac{z^+ (1-z^-)}{(z^+ + z^-)} e^{+ik_x x} \right) E_{IVb}^+. \quad (2.86)$$

Then, applying the boundary conditions at  $x = d$  and using (2.72), (2.85) and (2.86) we obtain

$$\left( \frac{z^- (1+z^+)}{(z^+ + z^-)} e^{-ik_x d} + \frac{z^+ (1-z^-)}{(z^+ + z^-)} e^{+ik_x d} \right) E_{IVb}^+ = E_{IIb}^+ e^{-ik_{01} d} + E_{IIb}^- e^{+ik_{01} d}, \quad (2.87)$$

$$\left( \frac{1}{Z^-} \frac{z^- (1+z^+)}{(z^+ + z^-)} e^{-ik_x d} - \frac{1}{Z^+} \frac{z^+ (1-z^-)}{(z^+ + z^-)} e^{+ik_x d} \right) Z_1 E_{IVb}^+ = E_{IIb}^+ e^{-ik_{01} d} - E_{IIb}^- e^{+ik_{01} d}, \quad (2.88)$$

Eliminating  $E_{II}^+$  and  $E_{II}^-$  from each other and writing them in a separately it gives us

$$E_{IIb}^+ = \frac{1}{2} \left[ \frac{z^- (1+z^+)}{(z^+ + z^-)} \left( 1 + \frac{z_1}{z^-} \right) e^{-ik_x d} + \frac{z^+ (1-z^-)}{(z^+ + z^-)} \left( 1 - \frac{z_1}{z^+} \right) e^{+ik_x d} \right] E_{IVb}^+ e^{+ik_{01} d}, \quad (2.89)$$

$$E_{IIb}^- = \left( \frac{z^- (1+z^+)}{(z^+ + z^-)} \left[ 1 - \frac{1}{2} \left( 1 + \frac{z_1}{z^-} \right) \right] e^{-ik_x d} + \frac{z^+ (1-z^-)}{(z^+ + z^-)} \left[ 1 - \frac{1}{2} \left( 1 - \frac{z_1}{z^+} \right) \right] e^{+ik_x d} \right) E_{IVb}^+ e^{-ik_{01} d}. \quad (2.90)$$

Finally, applying the boundary condition (continuity of the tangential components of electric and magnetic fields in each respective region) at  $x = d + L$  and using (2.70)-(2.71) and (2.89)-(2.90),

$$E_{Ib}^+ e^{-ik_0(d+L)} + E_{Ib}^- e^{+ik_0(d+L)} = E_{IIb}^+ e^{-ik_{01}(d+L)} + E_{IIb}^- e^{+ik_{01}(d+L)}, \quad (2.91)$$

$$E_{Ib}^+ e^{-ik_0(d+L)} - E_{Ib}^- e^{+ik_0(d+L)} = \frac{1}{z_1} \left( E_{IIb}^+ e^{-ik_{01}(d+L)} - E_{IIb}^- e^{+ik_{01}(d+L)} \right), \quad (2.92)$$



$$2e^{-ik_0(d+L)} = \frac{E_{IIb}^+ \left(1 + \frac{1}{z_1}\right) e^{-ik_{01}(d+L)} + E_{IIb}^- \left(1 - \frac{1}{z_1}\right) e^{+ik_{01}(d+L)}}{E_{Ib}^+} \quad (2.93)$$

Dividing the fourth region forward electric field over first region forward electric field we obtain long equation of

$$\frac{E_{IVb}^+}{E_{Ib}^+} = \frac{2e^{-ik_0(d+L)}}{\left(1 + \frac{1}{z_1}\right) \left[ \left(1 + \frac{z_1}{z^-}\right) \Lambda_5 + \left(1 - \frac{z_1}{z^+}\right) \Lambda_6 \right] e^{-ik_{01}L} + \left(1 - \frac{1}{z_1}\right) \left[ \left(1 - \frac{z_1}{z^-}\right) \Lambda_5 + \left(1 + \frac{z_1}{z^+}\right) \Lambda_6 \right] e^{+ik_{01}L}}. \quad (2.94)$$

Therefore, using substituent of  $\Lambda_5$  and  $\Lambda_6$  remain us a little short equation,

$$\Lambda_5 = \frac{z^- (1 + z^+)}{2(z^+ + z^-)} e^{-ik_x d}, \quad \Lambda_6 = \frac{z^+ (1 - z^-)}{2(z^+ + z^-)} e^{+ik_x d}, \quad (2.95)$$

from here, we obtain the backward reflection S-parameter ( $S_{12}$ ) as

$$S_{12} = \frac{2}{\left(1 + \frac{1}{z_1}\right) \left[ \left(1 + \frac{z_1}{z^-}\right) \Lambda_5 + \left(1 - \frac{z_1}{z^+}\right) \Lambda_6 \right] e^{-ik_{01}L} + \left(1 - \frac{1}{z_1}\right) \left[ \left(1 - \frac{z_1}{z^-}\right) \Lambda_5 + \left(1 + \frac{z_1}{z^+}\right) \Lambda_6 \right] e^{+ik_{01}L}}. \quad (2.96)$$

## 2.4 Power Analysis

Firstly, we found all necessary relations about the electric field and magnetic fields. Therefore, here our main purpose is obtaining the exact complex power relation for each medium.

### For 1<sup>st</sup> Region:

Using the below equation for the electric and magnetic field intensity of first medium,

$$\vec{E}_I = \hat{a}_z \left( E_I^+ e^{ik_0x} + E_I^- e^{-ik_0x} \right), \quad (2.97)$$

$$\vec{H}_I = \hat{a}_y \frac{1}{Z_0} \left( -E_I^+ e^{ik_0x} + E_I^- e^{-ik_0x} \right), \quad (2.98)$$

General complex power relation is,

$$\vec{S}_I = \frac{1}{2} \vec{E}_I \times \vec{H}_I^* \quad (2.99)$$

From equation (2.97) and (2.98) we get

$$\vec{S}_I = \frac{1}{2} \hat{a}_z \left( E_I^+ e^{ik_0x} + E_I^- e^{-ik_0x} \right) \times \hat{a}_y \frac{1}{Z_0} \left( -E_I^{+*} e^{ik_0x} + E_I^{-*} e^{-ik_0x} \right), \quad (2.100)$$

Multiplying the equation (2.100) we get,

$$\vec{S}_I = -\frac{1}{2Z_0} \hat{a}_x \left( \begin{array}{l} -E_I^{+*} e^{ik_0x} E_I^+ e^{ik_0x} - E_I^{+*} e^{ik_0x} E_I^- e^{-ik_0x} \\ + E_I^{-*} e^{-ik_0x} E_I^+ e^{ik_0x} + E_I^{-*} e^{-ik_0x} E_I^- e^{-ik_0x} \end{array} \right). \quad (2.101)$$

Multiplication of complex variable with its conjugate always gives us magnitude of its square. Therefore,

$$\vec{S}_I = -\frac{1}{2Z_0} \hat{a}_x \left( -|E_I^+|^2 e^{2ik_0x} - E_I^{+*} E_I^- + E_I^{-*} E_I^+ + |E_I^-|^2 e^{-2ik_0x} \right) \quad (2.102)$$

Finally applying the boundary conditions at  $x = 0$ , we get

$$\vec{S}_I(x=0) = -\hat{a}_x \frac{1}{2Z_0} \left( |E_I^-|^2 - |E_I^+|^2 + E_I^{-*} E_I^+ - E_I^- E_I^{+*} \right), \quad (2.103)$$

When we run the Matlab code in appendix  $\vec{S}_I(x=0)$ . It gives the value of

$$\vec{S}_I(x=0) = 351.233344613523e-006 - 5.54801202230450e-003i.$$

As a consequence, eliminating the  $E_I^-$  in (2.103), with the S-parameter relation  $S_{11}$  leads to,

$$\vec{S}_I(x=0) = -\hat{a}_x \frac{1}{2Z_0} \left( |S_{11}|^2 + S_{11}^* - S_{11} - 1 \right) |E_I^+|^2, \quad E_I^- = S_{11} E_I^+. \quad (2.104)$$

**For 2<sup>nd</sup> region:**

Using the below equation (2.105) and (2.106) belongs to the electric and magnetic field intensity of second medium,

$$\vec{E}_{II} = \hat{a}_z \left( E_{II}^+ e^{ik_x x} + E_{II}^- e^{-ik_x x} \right), \quad (2.105)$$

$$\vec{H}_{II} = \hat{a}_y \left( -\frac{E_{II}^+}{Z^+} e^{ik_x x} + \frac{E_{II}^-}{Z^-} e^{-ik_x x} \right), \quad (2.106)$$

General complex power relation for second medium is

$$\vec{S}_{II} = \frac{1}{2} \vec{E}_{II} \times \vec{H}_{II}^* \quad (2.107)$$

$$\bar{S}_{II} = \frac{1}{2} \hat{a}_z \left( E_{II}^+ e^{ik_x x} + E_{II}^- e^{-ik_x x} \right) \times \hat{a}_y \left( -\frac{E_{II}^{+*}}{Z^{+*}} e^{ik_x x} + \frac{E_{II}^{-*}}{Z^{-*}} e^{-ik_x x} \right), \quad (2.108)$$

The equation (2.108) can be written as,

$$\bar{S}_{II} = \frac{1}{2} \bar{E}_{II} \times \bar{H}_{II}^* = -\frac{1}{2} \hat{a}_x \left( \begin{array}{l} -\frac{1}{Z^{+*}} |E_{II}^+|^2 e^{i(k_x - k_x^*)x} + \frac{E_{II}^{-*}}{Z^{-*}} E_{II}^+ e^{i(k_x + k_x^*)x} \\ -\frac{E_{II}^{+*}}{Z^{+*}} E_{II}^- e^{-i(k_x + k_x^*)x} + \frac{1}{Z^{-*}} |E_{II}^-|^2 e^{-i(k_x - k_x^*)x} \end{array} \right), \quad (2.109)$$

Applying the boundary conditions at  $x = d_1$ , we get

$$\bar{S}_{II}(x = d_1) = -\frac{1}{2Z_0} \hat{a}_x \left( \begin{array}{l} -\frac{1}{z^{+*}} |E_{II}^+|^2 e^{i(k_x - k_x^*)d_1} + \frac{E_{II}^{-*}}{z^{-*}} E_{II}^+ e^{i(k_x + k_x^*)d_1} \\ -\frac{E_{II}^{+*}}{z^{+*}} E_{II}^- e^{-i(k_x + k_x^*)d_1} + \frac{1}{z^{-*}} |E_{II}^-|^2 e^{-i(k_x - k_x^*)d_1} \end{array} \right), \quad (2.110)$$

Writing the propagation constant  $k_x$  with a refractive index  $n$  which is  $k_x = nk_0$ .

$$\bar{S}_{II}(x = d_1) = -\frac{1}{2Z_0} \hat{a}_x \left( \begin{array}{l} -\frac{1}{z^{+*}} |E_{II}^+|^2 e^{+ik_0(n_{bian} - n^*)d_1} + \frac{E_{II}^{-*}}{z^{-*}} E_{II}^+ e^{+ik_0(n_{bian} + n^*)d_1} \\ -\frac{E_{II}^{+*}}{z^{+*}} E_{II}^- e^{-ik_0(n_{bian} + n^*)d_1} + \frac{1}{z^{-*}} |E_{II}^-|^2 e^{-ik_0(n_{bian} - n^*)d_1} \end{array} \right), \quad (2.111)$$

Finally, our result leads to

$$\vec{S}_{II}(x=d_1) = -\frac{1}{2Z_0} \hat{a}_x \left( \begin{array}{l} -\frac{1}{z^{+*}} |E_{II}^+|^2 e^{-2k_0 \text{Im}\{n_{bian}\}d_1} + \frac{1}{z^{-*}} |E_{II}^-|^2 e^{+2k_0 \text{Im}\{n_{bian}\}d_1} \\ + E_{II}^+ \frac{E_{II}^{-*}}{z^{-*}} e^{+i2k_0 \text{Re}\{n_{bian}\}d_1} - E_{II}^- \frac{E_{II}^{+*}}{z^{+*}} e^{-i2k_0 \text{Re}\{n_{bian}\}d_1} \end{array} \right), \quad (2.112)$$

When we run the Matlab code in appendix  $\vec{S}_{II}(x=d_1)$ . It gives the value of

$$\vec{S}_{II}(x=d_1) = 7.82513704347104\text{e-}006 - 491.612244953627\text{e-}009i.$$

Again applying the boundary conditions at  $x=0$  for second region for validation, we get

$$\vec{S}_{II}(x=0) = -\hat{a}_x \frac{1}{2Z_0} \left( \begin{array}{l} \frac{|E_{II}^-|^2}{z^{-*}} - \frac{|E_{II}^+|^2}{z^{+*}} + \frac{E_{II}^{-*}}{z^{-*}} E_{II}^+ - \frac{E_{II}^{+*}}{z^{+*}} E_{II}^- \end{array} \right), \quad (2.113)$$

In equation (2.113) eliminating  $E_{II}^-$  and leave alone  $E_{II}^+$  gives

$$\vec{S}_{II}(x=0) = -\hat{a}_x \frac{1}{2} \left( \frac{|\Lambda_3|^2}{Z^{-*}} - \frac{1}{Z^{+*}} + \frac{\Lambda_3^*}{Z^{-*}} - \frac{\Lambda_3}{Z^{+*}} \right) |E_{II}^+|^2, \quad E_{II}^- = \Lambda_3 E_{II}^+. \quad (2.114)$$

To present (2.114) with  $E_I^+$  and  $\Lambda_3$ , we obtain

$$\vec{S}_{II}(x=0) = -\hat{a}_x \frac{1}{2} \left( \frac{|\Lambda_3|^2}{Z^{-*}} - \frac{1}{Z^{+*}} + \frac{\Lambda_3^*}{Z^{-*}} - \frac{\Lambda_3}{Z^{+*}} \right) \left| \frac{2}{\left[ -\frac{Z_0}{Z^+} + \frac{Z_0}{Z^-} \Lambda_3 - (1 + \Lambda_3) \right]} \right|^2 |E_I^+|^2. \quad (2.115)$$

When we run the Matlab code in appendix  $\vec{S}_{II}(x=0)$ . It gives the value of

$$\vec{S}_{II}(x=0) = 351.233344613524\text{e-}006 - 5.54801202230450\text{e-}003i.$$

Here we derive electric and magnetic field intensity equations with the relation  $\Lambda$  parameter. Let us write for second region,

$$\begin{pmatrix} \vec{E}_{II} = \hat{a}_z E_{II}^+ \left( e^{ik_x x} + \Lambda_3 e^{-ik_x x} \right) \\ \vec{H}_{II} = \hat{a}_y E_{II}^+ \left( -\frac{1}{Z^+} e^{ik_x x} + \frac{\Lambda_3}{Z^-} e^{-ik_x x} \right) \end{pmatrix}, \quad (2.116)$$

for the first region it has

$$\begin{pmatrix} \vec{E}_I = \hat{a}_z \left( E_I^+ e^{ik_0 x} + E_I^- e^{-ik_0 x} \right) \\ \vec{H}_I = \hat{a}_y \frac{1}{Z_0} \left( -E_I^+ e^{ik_0 x} + E_I^- e^{-ik_0 x} \right) \end{pmatrix}. \quad (2.117)$$

Incorporating the (2.116) and (2.117) and leads to

$$\begin{pmatrix} E_{II}^+ (1 + \Lambda_3) - E_I^+ = E_I^- \\ E_{II}^+ \left( -\frac{Z_0}{Z^+} + \frac{Z_0}{Z^-} \Lambda_3 \right) = -E_I^+ + E_I^- \end{pmatrix}. \quad (2.118)$$

Finally, we can write  $E_{II}^+$  and  $E_I^+$  in a single equation which is,

$$E_{II}^+ = -\frac{2}{\left[ -\frac{Z_0}{Z^+} + \frac{Z_0}{Z^-} \Lambda_3 - (1 + \Lambda_3) \right]} E_I^+ \quad (2.119)$$

**For 3<sup>rd</sup> Region:**

Let us obtain general complex power relation for third medium

$$\left( \begin{array}{l} \bar{S}_{III} = \frac{1}{2} \bar{E}_{III} \times \bar{H}_{III}^* = \\ -\frac{1}{2Z_1^*} \hat{a}_x \left( E_{III}^+ e^{ik_0 x} + E_{III}^- e^{-ik_0 x} \right) \left( -E_{III}^{+*} e^{-ik_0^* x} + E_{III}^{-*} e^{+ik_0^* x} \right), \end{array} \right) \quad (2.120)$$

Writing the equation of (2.120) with a function of thickness gives us

$$\bar{S}_{III}(x) = -\frac{1}{2Z_1^*} \hat{a}_x \left( \begin{array}{l} +|E_{III}^-|^2 e^{+ik_0(n^*-n)x} - |E_{III}^+|^2 e^{ik_0(n-n^*)x} \\ +E_{III}^+ E_{III}^{-*} e^{+ik_0(n^*+n)x} - E_{III}^- E_{III}^{+*} e^{-ik_0(n+n^*)x} \end{array} \right). \quad (2.121)$$

Applying the boundary conditions at  $x = d$  for third region for validation, we get

$$\bar{S}_{III}(x=d) = -\frac{1}{2Z_1^*} \hat{a}_x \left( \begin{array}{l} +|E_{III}^-|^2 e^{-ik_0(n-n^*)d} - |E_{III}^+|^2 e^{+ik_0(n-n^*)d} \\ +E_{III}^+ E_{III}^{-*} e^{+ik_0(n+n^*)d} - E_{III}^- E_{III}^{+*} e^{-ik_0(n+n^*)d} \end{array} \right). \quad (2.122)$$

Moreover, if we use complex mathematical properties

$$\left( \begin{array}{l} (n-n^*) = 2 \operatorname{Im}\{n\} \\ (n+n^*) = 2 \operatorname{Re}\{n\} \end{array} \right) \quad (2.123)$$

And then, if we incorporate the equation of (2.122) and (2.123), it leads to

$$\bar{S}_{III}(x=d) = -\frac{1}{2Z_1^*} \hat{a}_x \left( \begin{array}{l} |E_{III}^-|^2 e^{+2k_0 \operatorname{Im}\{n\}d} - |E_{III}^+|^2 e^{-2k_0 \operatorname{Im}\{n\}d} \\ +E_{III}^+ E_{III}^{-*} e^{+2ik_0 \operatorname{Re}\{n\}d} - E_{III}^- E_{III}^{+*} e^{-2ik_0 \operatorname{Re}\{n\}d} \end{array} \right). \quad (2.124)$$

When we run the Matlab code in appendix  $\bar{S}_{III}(x=d)$ . It gives the value of

$$\vec{S}_{III}(x=d) = 7.82513704347104e-006 - 491.612244953630e-009i .$$

Finally power relation of third region at  $x = d + L$  can be written from the equation (2.124) just changing the thickness parameter 'd'.

$$\vec{S}_{III}(x=d+L) = -\frac{1}{2Z_1^*} \hat{a}_x \left( \begin{array}{l} |E_{III}^-|^2 e^{+2k_0 \text{Im}\{n\}(d+L)} - |E_{III}^+|^2 e^{-2k_0 \text{Im}\{n\}(d+L)} \\ + E_{III}^+ E_{III}^-^* e^{+2ik_0 \text{Re}\{n\}(d+L)} - E_{III}^- E_{III}^+^* e^{-2ik_0 \text{Re}\{n\}(d+L)} \end{array} \right). \quad (2.125)$$

When we run the Matlab code in appendix  $\vec{S}_{III}(x=d+L)$ . It gives the value of

$$\vec{S}_{III}(x=d+L) = 800.138543394125e-009 + 13.2348898008484e-024i.$$



**For 4<sup>th</sup> Region:**

The last our purpose is obtaining the power relation of fourth region. Since there is no boundary at the end of the region so that we can calculate it easily,

$$\bar{S}_4(x = d + L) = \frac{1}{2}(\bar{E}_{IV} X \bar{H}_{IV}^*). \quad (2.126)$$

Incorporating the (2.39) and (2.40) equation into the (2.126)

$$\bar{S}_4 = \frac{1}{2}(\hat{a}_z E_{IV}^+ e^{ik_0 x}) X \left( -\hat{a}_y \frac{1}{Z_0} E_{IV}^{+*} e^{-ik_0 x} \right), \quad (2.127)$$

from (2.127), as you below see  $\bar{S}_4$  is independent from the thickness 'd' ,

$$\bar{S}_4 = \frac{\hat{a}_x}{2Z_0} (E_{IV}^+ E_{IV}^{+*} e^{ik_0 x} e^{-ik_0 x}). \quad (2.128)$$

Finally,  $\bar{S}_4$  simplifies into the

$$\bar{S}_4(x = d + L) = \frac{\hat{a}_x}{2Z_0} (|E_{IV}^+|^2). \quad (2.129)$$

When we run the Matlab code in appendix  $\bar{S}_4(x = d + L)$ . It gives the value of

$$\bar{S}_4(x = d + L) = 800.138543394125e-009.$$

## CHAPTER 3

### NUMERICAL ANALYSIS OF PROPAGATION CHARACTERISTICS OF A COMPOSITE MATERIAL WITH A BI-ANISOTROPIC SLAB AND A CONVENTIONAL MATERIAL

#### 3.1 Introduction

In the previous chapter, we focused on the derivation of expression for forward and backward reflection and transmission scattering (S-) parameters of a composite material with a bi-anisotropic metamaterial slab and a conventional material. In addition, we also obtained expressions for transmitted, reflected and loss behavior to investigate its propagation characteristics. In this chapter, we turn our attention to validation of the derived expressions in the previous chapter. We perform a numerical analysis to achieve our goal. In the analysis, we use Lorentz dispersion models to simulate artificial bi-anisotropic slab and the conventional material as well as to analyze the propagation characteristics of the composite material. In addition to this model we utilized transfer matrix method, which is an appropriate method for analysis of cascaded structures, to validate derived expressions.

### 3.2 Lorentz Model

Lorentz medium is a frequency dispersive medium in which the permittivity and permeability of the material are the function of the frequency. These materials have resonance phenomena caused by the oscillation of the electron and nuclei subject to an applied field. Lorentz was the first to study such phenomena when developing the theory of the electron. The model conceptually replaces the atoms and molecules of a real material by a set of harmonically bound electron oscillators, resonant at some frequency  $\omega_0$ . At frequencies far below  $\omega_0$ , an applied electric field displaces the electrons from the positive core, inducing a polarization in the same direction as the applied electric field. At frequencies near the resonance, the induced polarization becomes very large, as is typically the case in resonance phenomena; the large response represents accumulation of energy over many cycles, such that a considerable amount of energy is stored in the medium relative to the driving field. So large is this stored energy that even changing the sign of the applied electric field has little effect on the polarization near resonance. That is, as the frequency of the driving electric field is swept through the resonance, the polarization flips from in-phase to out-of-phase with the driving field and the material exhibits a negative response. If instead of electrons the material response were due to harmonically bound magnetic moments, then a negative magnetic response would exist. Though somewhat less common than positive materials, negative materials are nevertheless easy to find. Materials with  $\epsilon$  negative include metals (e.g., silver, gold, aluminum) at optical frequencies, while materials with  $\mu$  negative include resonant ferromagnetic or antiferromagnetic systems [32, 33]. As a result, the shape of the dispersive components of the material parameters for DNG metamaterial can be described by using Lorentz medium model.

To model the dispersive behaviour of bianisotropic MM slabs, we consider the following expressions based on Lorentzian model [34-36]

$$\epsilon_z(f) = 1 - \frac{F_e f^2}{f^2 - f_e^2 + i\gamma_e f}, \quad \mu_y(f) = 1 - \frac{F_m f^2}{f^2 - f_m^2 + i\gamma_m f}, \quad (3.1)$$

$$\xi_0(f) = 1 - \frac{F_\xi f^2}{f^2 - f_\xi^2 + i\gamma_\xi f}. \quad (3.2)$$

Here,  $f_e$ ,  $f_m$ , and  $f_\xi$  are electric, magnetic, and magneto-electric resonance frequencies;  $\gamma_e$ ,  $\gamma_m$ , and  $\gamma_\xi$  are electric, magnetic, and magneto-electric damping frequencies; and  $F_e$ ,  $F_m$ , and  $F_\xi$  coefficients depending on structure of the material [34]. Lorentz Model can be applied for both conventional materials and metamaterials problems.

### 3.3 Transfer Matrix Method

The transfer matrix method (TMM) is a method used in optics and acoustics to analyze the propagation of electromagnetic or acoustic waves through a stratified (layered) medium [37]. TMM is based on the fact that, according to Maxwell's equations, there are simple continuity conditions for the electric field across boundaries from one medium to the next. If the field is known at the beginning of a layer, the field at the end of the layer can be derived from a simple matrix operation. A stack of layers can then be represented as a system matrix, which is the product of the individual layer matrices. The final step of the method involves converting the system matrix back into reflection and transmission coefficients [38].

TMM is a powerful tool for the analysis of periodic structures. It has been used in two different ways. One way is to represent the solution of the coupled mode equations by a  $2 \times 2$  transfer matrix, which relates the forward and backward propagating field amplitudes [34]. Almost-periodic gratings can be analyzed effectively by this method [38]. The grating structure is divided into a number of uniform grating sections which have an analytic transfer matrix. The transfer matrix for the entire structure can be obtained by multiplying the individual transfer matrices together. It should be noted that this method is simply a numerical method for solving the coupled mode equations.

The other way of the TMM is to represent each corrugation section by a transfer matrix [39, 29]. The reflection of the propagating modes of a corrugated waveguide at the discontinuity of the effective index in the same way as plane waves are

reflected. Therefore, the transfer matrix of each corrugation section can be expressed in terms of the mode reflection and transmission coefficients and the propagation constant, which is similar to the matrix used in the analysis of thin-film optical filters [40].

Let us try to find TMM of whole multilayer structure through the multiplication of cascaded connection of each layer in Figure 3.1 by,

$$[M_t] = \begin{bmatrix} m_{11}^t & m_{12}^t \\ m_{21}^t & m_{22}^t \end{bmatrix} = \prod_{s=1}^N [M_s] = \prod_{s=1}^N \begin{bmatrix} m_{11}^s & m_{12}^s \\ m_{21}^s & m_{22}^s \end{bmatrix}, \quad (3.3)$$

where  $m_{11}^t$ ,  $m_{12}^t$ ,  $m_{21}^t$ , and  $m_{22}^t$  designate the elements of  $M_t$ , and  $M_s$  denotes the transfer matrix of any layer and is written as

$$\begin{bmatrix} m_{11}^s & m_{12}^s \\ m_{21}^s & m_{22}^s \end{bmatrix} = \begin{bmatrix} \frac{(1+S_{11})(1-S_{22})+S_{21}S_{12}}{2S_{21}} & \frac{(1+S_{11})(1+S_{22})-S_{21}S_{12}}{2S_{21}} \\ \frac{(1-S_{11})(1-S_{22})-S_{21}S_{12}}{2S_{21}} & \frac{(1-S_{11})(1+S_{22})+S_{21}S_{12}}{2S_{21}} \end{bmatrix}. \quad (3.4)$$

Forward and backward reflection and transmission S-parameters of a bianisotropic MM slab with length  $L$  [41] are

$$S_{11} = \frac{\Gamma_1(1-T^2)}{1-\Gamma_1\Gamma_2T^2}, \quad S_{22} = \frac{\Gamma_2(1-T^2)}{1-\Gamma_1\Gamma_2T^2}, \quad S_{21} = S_{12} = \frac{(1-\Gamma_1\Gamma_2)T}{1-\Gamma_1\Gamma_2T^2}, \quad (3.5)$$

$$\Gamma_{(1,2)} = \frac{z_w^{+(-)} - 1}{z_w^{+(-)} + 1}, \quad z_w^+ = \frac{\mu_z}{n \mp i\xi_0}, \quad T = e^{+ik_0nL}, \quad n = \mp \sqrt{\epsilon_r\mu_r - \xi_0^2}. \quad (3.6)$$

Here,  $\Gamma_1$  and  $\Gamma_2$  are the intrinsic (first) reflection coefficients at the interfaces of front and back faces of each MM slab;  $T$  is the propagation factor related to

propagation characteristics of the slabs;  $z_w^+$ ,  $z_w^-$ ,  $n$ , and  $k_0$  are, respectively, the normalized wave impedances in forward (+x) and backward (-x) directions, the refractive index of each bi-anisotropic MM slab, and the free-space wave number;  $\epsilon_r$  and  $\mu_r$  are the relative complex permittivity and complex permeability of bianisotropic MM slab in electric and magnetic field directions, respectively; and  $\xi_0$  is the magneto-electric coupling coefficient (a unitless quantity).

For a conventional material ( $n > 0$ ), its expressions for  $S_{11}$ ,  $S_{21}$ ,  $S_{12}$ ,  $S_{22}$  are identical (correspondingly) to those in equation (3.5) if  $\xi_0 = 0$ . Therefore, its expressions are not repeated for convenience.

After determining  $[M_t]$  through equation (3.3), expressions of  $P_r$ ,  $P_t$ , and  $P_l$  normalized to incident power can be calculated from [42,43-45]

$$P_r^{(1)} = \left| \frac{m_{11}^t + m_{12}^t - m_{21}^t - m_{22}^t}{m_{11}^t + m_{12}^t + m_{21}^t + m_{22}^t} \right|^2, \quad P_r^{(2)} = \left| \frac{m_{22}^t + m_{12}^t - m_{21}^t - m_{11}^t}{m_{11}^t + m_{12}^t + m_{21}^t + m_{22}^t} \right|^2, \quad (3.7)$$

$$P_t = \left| \frac{2}{m_{11}^t + m_{12}^t + m_{21}^t + m_{22}^t} \right|^2, \quad P_l^{(1,2)} = 1 - P_r^{(1,2)} - P_t, \quad (3.8)$$

where  $\{P_r^{(1)}, P_l^{(1)}\}$  and  $\{P_r^{(2)}, P_l^{(2)}\}$  are, respectively, pairs of normalized reflected and loss powers from forward and backward directions of the cascaded structure in Figure 3.1. We note that because of the reflection asymmetric property of bianisotropic MM slabs,  $P_r^{(1)}$  and  $P_r^{(2)}$  (as well as  $P_l^{(1)}$  and  $P_l^{(2)}$ ) should be different. This point is discussed in what follows by numeric examples.

### 3.4 Validation of S-Parameters by Transfer Matrix Method (TMM) and Lorentzian Model

In Chapter 2, the value of  $S_{11}$ ,  $S_{21}$ ,  $S_{12}$  and  $S_{22}$  parameters have been found analytically, and here in this section we numerically validate these parameters. We

achieve this validation of S-parameters using Transfer Matrix Method and Lorentzian model (analytical and numerical). To compare two methods we analyze the magnitude and phase of S - parameters for a frequency range of 0 and 25 GHz. As a particular example, we consider the Lorentzian model parameters discussed previous section as

$$F_e = F_m = 0.4, \quad F_\xi = 0.15, \quad (3.9)$$

$$f_e = 6 \text{ GHz}, \quad f_m = f_\xi = 5 \text{ GHz}, \quad (3.10)$$

$$\gamma_e = \gamma_m = \gamma_\xi = 0.4 \text{ GHz}. \quad (3.11)$$

Here, we note that there is no specific reason of the selection of above parameters. Our purpose is just simulating constitutive parameters of the bianisotropic MM slab for validation of derivation.

### 3.4.1 Validation of $S_{11}$

As seen from Figure 3.2, the magnitude and phase of forward reflection scattering parameter ( $S_{11}$ ) determined from the TMM method and analytical derivation Equation (2.51) are almost equal to each other. This validates our derivations in Chapter 2 for  $S_{11}$ . As you see frequency of resonance about 5-6 GHz is clearly seen in both magnitude and phase figures.

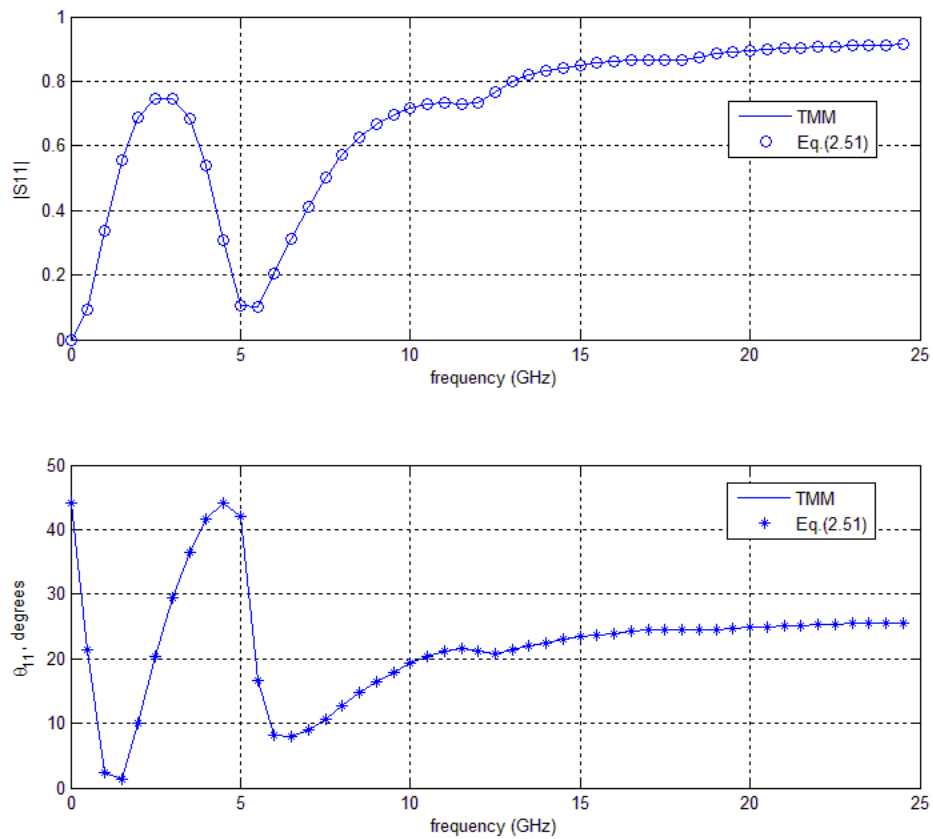


**Figure 3.1:** Dependencies of magnitudes and phases of forward reflection scattering parameter  $S_{11}$ .



### 3.4.2 Validation of $S_{21}$

Here, in Figure 3.3 we compare the magnitude and phase of forward transmission coefficient of  $S_{21}$  parameter. By using Transfer Matrix Method and Equation (2.69).

Therefore, our second validation of  $S_{21}$  is done well.

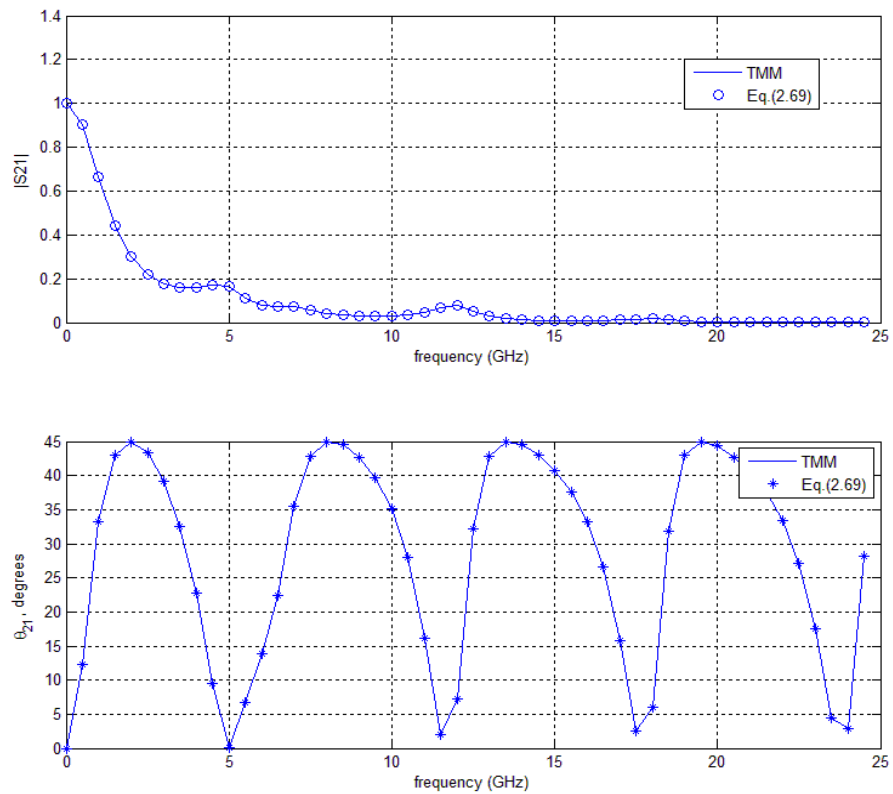


**Figure 3.2:** Dependencies of magnitudes and phases of forward reflection scattering parameter  $S_{21}$ .

### 3.4.3 Validation of $S_{12}$

Here, in Figure 3.4 we compare the magnitude and phase of backward transmission coefficient of  $S_{12}$  parameter. As we analyze the figures of TMM method and Equation (2.96) distinctly they are totally the same with each other so that our third validation of  $S_{12}$  is done correctly. However, when we compare the backward transmission coefficient of  $S_{12}$  parameter and forward transmission coefficient of  $S_{21}$  parameter they are also the same with each other.

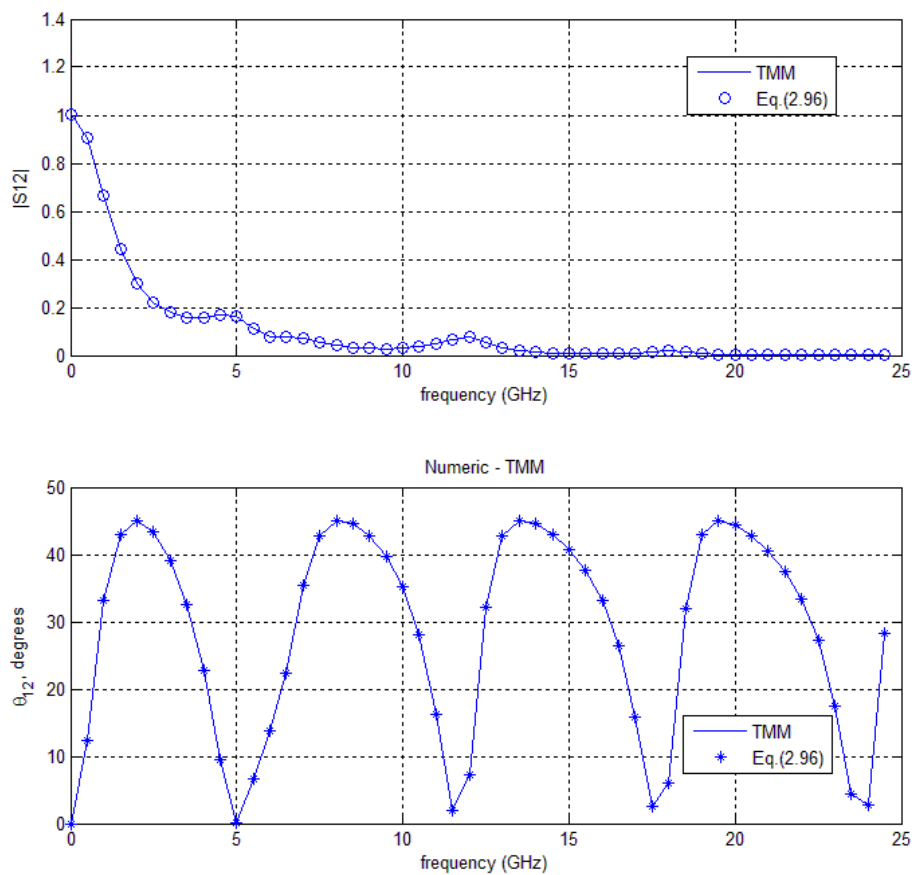


**Figure 3.3:** Dependencies of magnitudes and phases of forward reflection scattering parameter  $S_{12}$ .

### 3.4.4 Validation of $S_{22}$

In Figure 3.5, we compare the magnitude and phase of backward transmission coefficient of  $S_{22}$  parameter. When we look at the figures of TMM method and Equation (2.81) distinctly they are totally the same with each other so that our last validation of  $S_{22}$  is done correctly. However, when we compare the forward reflection coefficient of  $S_{11}$  parameter and backward reflection coefficient of  $S_{22}$  parameter they are completely different from each other.

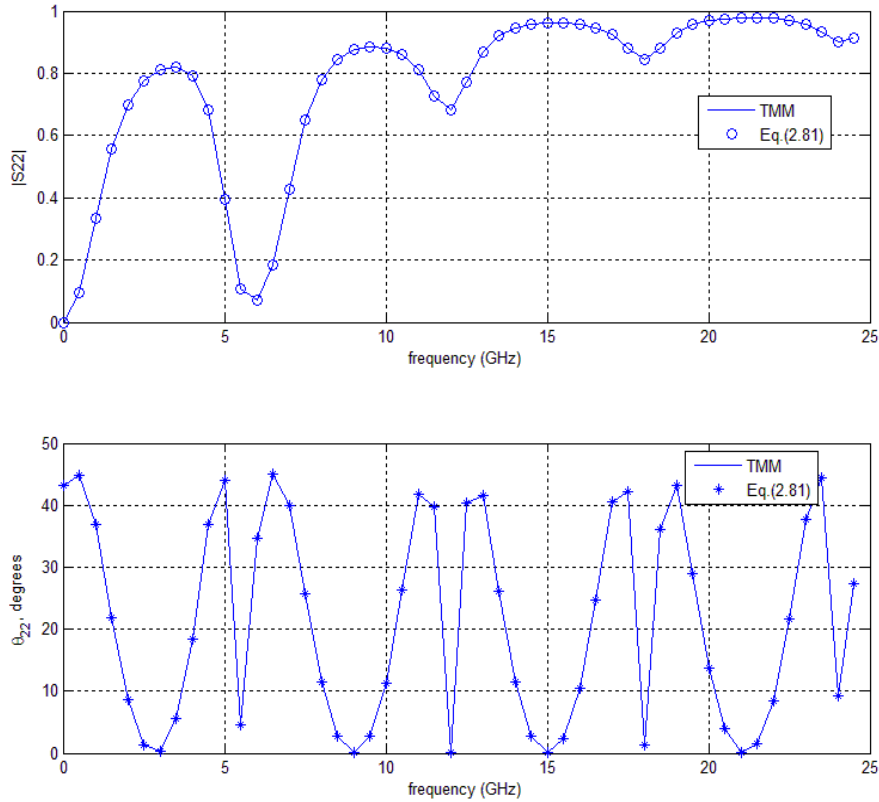


**Figure 3.4:** Dependencies of magnitudes and phases of forward reflection scattering parameter  $S_{22}$ .

As a result, we note the following two key points for the bianisotropic metamaterial property. First, bi-anisotropy property is symmetric to the transmission coefficient, and as a second bi-anisotropy shows an asymmetric property for the reflection coefficient.

### 3.5 Power Analysis

Here, we present numerical results of a two layer multilayer structure to demonstrate dependencies of reflection, transmission, and loss powers of a general multilayer structure in Figure 3.1. The results are separated into two subsections for better presentation. In the first subsection, we analyze aforementioned powers when the conventional material is lossless and when the bianisotropic MM slabs are low-loss. In the second subsection, we investigate effects of loss present both inside the conventional material and bianisotropic MM slab. In each subsection, we also investigate the effect of sample thickness on the analyzed powers.

#### 3.5.1 Low – Loss Case

Towards this end, as a particular example, we choose the Lorentzian model parameters discussed previous section as in equation (3.9) - (3.11). We also set  $\epsilon_r = 6.0 + i0.0$ ,  $\mu_r = 1.0 + i0.0$  for the conventional material and  $L_1 = L_2 = 10.0\text{mm}$ . For example, Figure 3.6 and 3.7 illustrate the dependencies of various reflected, transmitted, and loss powers for the analyzed two-layer structure for different  $L_1$  and  $L_2$  combinations over 0-25 GHz.

From the dependencies in Figure 3.6 and Figure 3.7, we note the following points. First, while the transmitted powers obtained from forward and backward directions of bianisotropic metamaterial slab are individually the same (Figures 3.6(c), 3.6(d) and Figures 3.7(c), 3.7(d)). The corresponding reflected and loss powers of each slab are different (Figures 3.6(a), 3.6(b), 3.6(e), 3.6(f) and Figures 3.7(a), 3.7(b), 3.7(e), 3.7(f)). For instance, whereas forward transmitted and backward transmitted are the same for bianisotropic MM slab, forward reflected and backward reflected powers are different for bianisotropic MM slab. The identical transmitted powers are a result of reciprocal property of each medium constituting the multilayer structure [25, 46, 47], and different reflected (and loss) powers comes from the reflection asymmetric ( $S_{11} \neq S_{22}$ ) nature of bianisotropic MM slabs (see Equation (3.7) and (3.8)). Second, reflected and transmitted powers of the conventional material demonstrate the oscillatory behavior over frequency ( Figures 3.6.(a), 3.6.(b), 3.6.(e), 3.6.(f) and

Figures 3.7(a), 3.7(b), 3.7(e), 3.7(f) ). This oscillatory behavior of the conventional material arises from its lossless nature ( $\text{Im}\{\epsilon_r\} = 0$  and  $\text{Im}\{\mu_r\} = 0$ ).

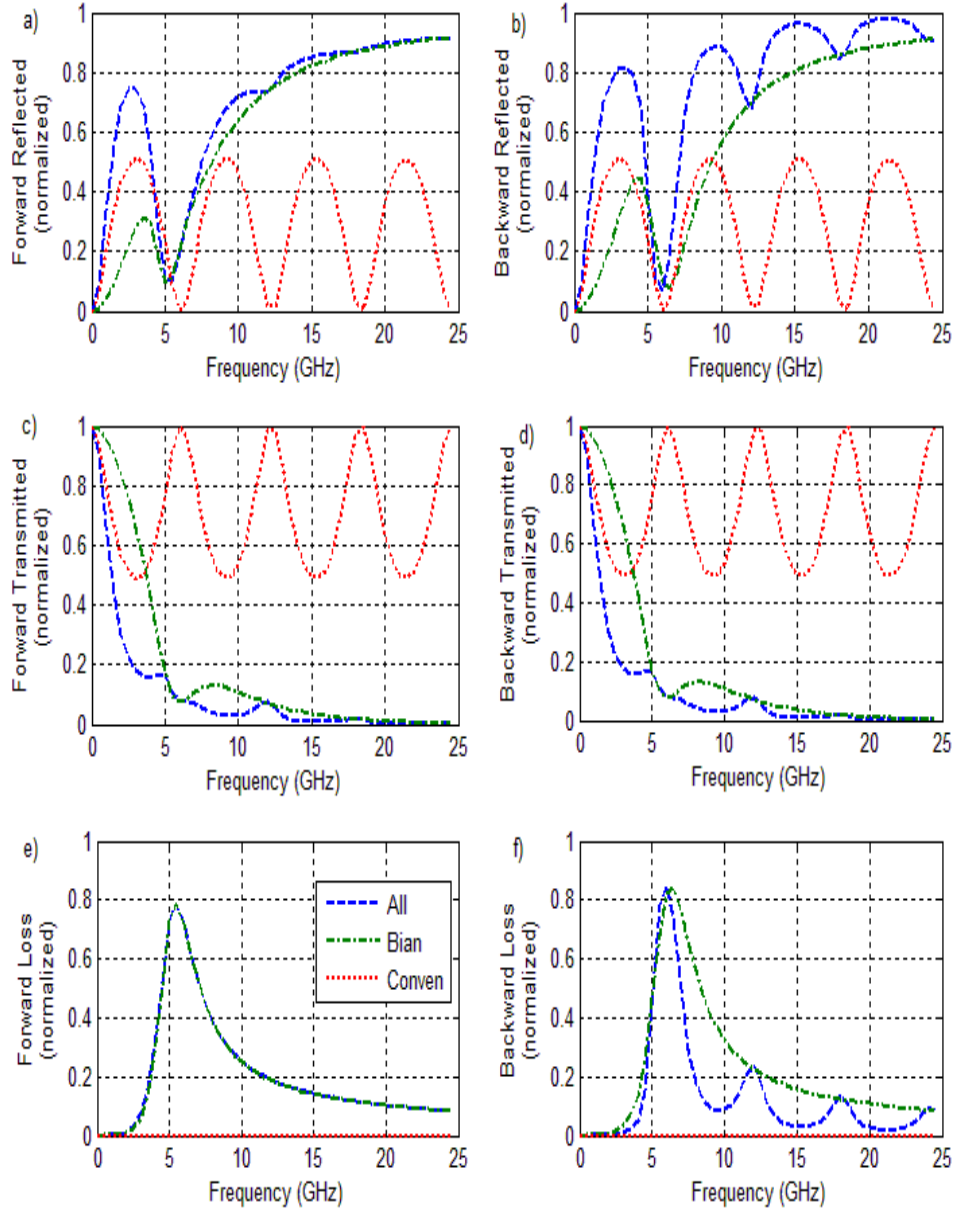


**Figure 3.5:** Dependencies of a) and b) reflected powers, c) and d) transmitted powers, e) and f) loss powers of the two-layer composite structure ( $L_1=L_2=10$  mm ).

Third, transmitted power of the composite structure possesses a null value around resonance frequencies  $f_e, f_m$ , and  $f_\xi$  ( Figures 3.6(c), 3.6(d) and Figures 3.7(c), 3.7(d)), indicating the common property of materials that electromagnetic energy is absorbed by the material at resonance [30]. In addition, transmitted (or reflected) power has a sharp peak at some specific frequencies (e.g.,  $f \cong 13.7$  GHz in Figures 3.6(a), 3.6(b), 3.6(c), and 3.6(d) ) beyond these resonance frequencies. These peaks corresponding to thickness-resonance frequencies of the conventional material. At those frequencies, the conventional material demonstrates maximum reflection property [48,49].

Fourth, the occurrence of peaks in reflected power increases (see Figures 3.6(c), 3.6(d) and Figures 3.7(c), 3.7(d)), with  $L_2$  due to increased oscillatory behavior of the conventional material. Therefore, resonance behavior at  $f \cong 13.7$  GHz and  $f \cong 19.9$  GHz in Figures 3.6(a), 3.6(b)) (or additional frequencies in Figures 3.7(a), 3.7(b)) can be utilized for sensing applications of the conventional materials [50, 51].

Fifth, total loss powers (Figures 3.6(e), 3.6(f), and Figure 3.7(e), 3.7(f),) increase drastically around resonance frequencies  $f_e, f_m$ , and  $f_\xi$  ( Figures 3.6(e), 3.6(f) and Figures 3.7(e), 3.7(f)), as well as at some specific frequencies resulting in a decreased reflected powers (e.g.,  $f \cong 13.7$  GHz and  $f \cong 19.9$  GHz in Figures 3.6(a), 3.6(b). Finally, we note from Figures 3.6(a), 3.6(b), 3.7(a), and 3.7(b) that forward and backward reflected and loss powers are, respectively, different from each other over the regions at which bianisotropic feature becomes a key parameter. For instance, the effect of  $\xi_0$  parameters is predominant over  $f \cong 5-7$  GHz in Figure 3.6 and Figure 3.7 [41, 52].

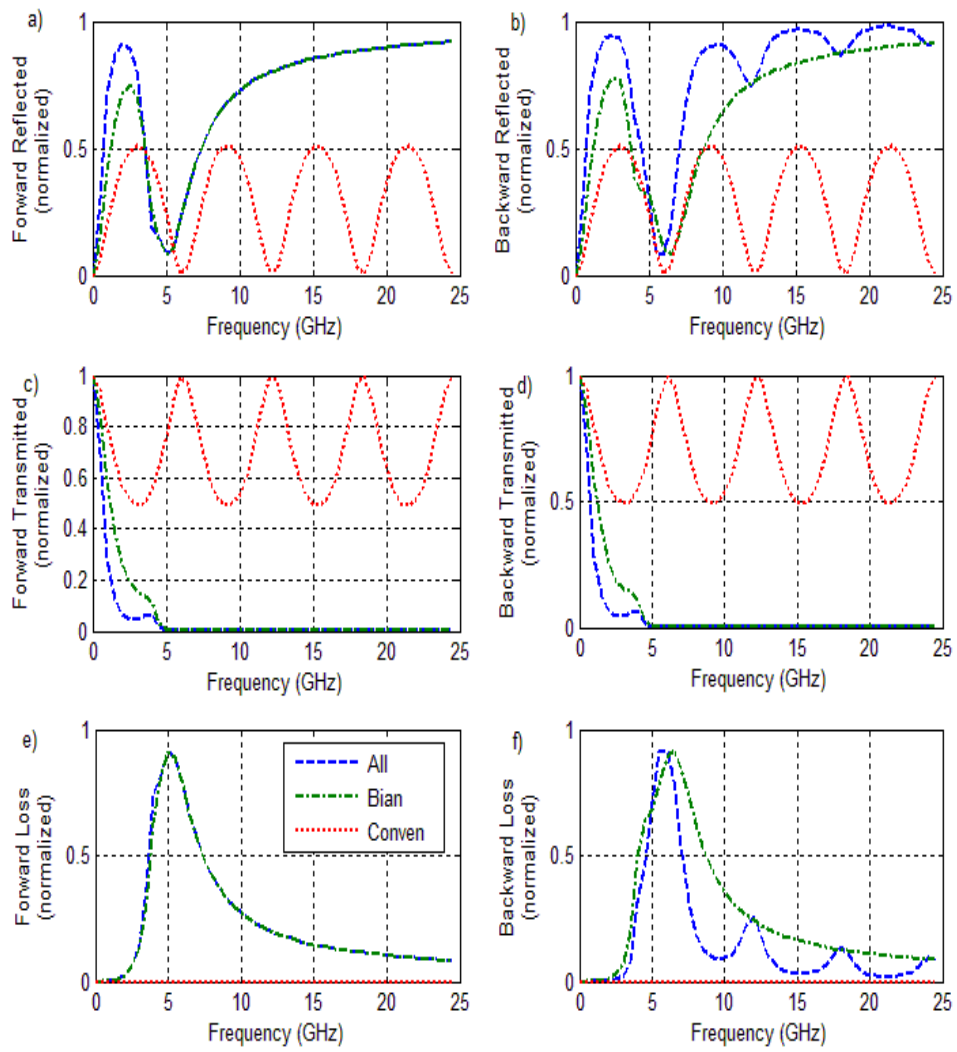


**Figure 3.6:** Dependencies of a) and b) reflected powers, c) and d) transmitted powers, e) and f) loss powers of the two-layer composite structure ( $L_1=40$ .mm,  $L_2=10$ .mm ).

### 3.5.2 Lossy Case

In the previous subsection, we investigated the transmitted, reflected, and loss powers of the two-layer composite structure in Figure 3.1 for low-loss bianisotropic MM slab and the lossless conventional material. Here, we mainly focus on the effects of increased loss inside both the bianisotropic MM slabs and the conventional material. In particular, we utilize following parameters to reflect losses inside the slabs

$$\gamma_e = \gamma_m = \gamma_\xi = 2.0 \text{ GHz} \quad (3.12)$$

while we keep other parameters the same in equations (3.9) and (3.10). For example Figure 3.8 and Figure 3.9 show the dependencies of  $P_t$ ,  $P_r$ , and  $P_l$  of the bianisotropic slab, the conventional material, and the analyzed multilayer structure for various  $\epsilon_r$  and  $\mu_r$  and thickness combinations. From these figures, we deduce the following points. First, the transmitted powers in forward and backward directions of the multilayer structure in Figures 3.8(c), 3.8(d), 3.9(c) and 3.9(d) are still the same. This is because reciprocity of a medium is not a parameter depending on the loss factor of the medium. Second, discrepancy of different reflected and loss powers in forward and backward directions of the multilayer structure still holds when the loss is included into the analysis (Figures 3.8(a), 3.8(b), 3.9(a) and 3.9(b)). This is because reflection asymmetric feature ( $S_{11} \neq S_{22}$ ) of the bianisotropic metamaterial slabs (producing the reflection asymmetric feature for the multilayer structure) is an intrinsic asymmetric nature of the physical constituents (e.g., orientation of metallic inclusions) [25, 30, 53], and because loss powers are related to reflected powers through the relation in (3.8). Third, the loss in the bianisotropic slab in addition to that in the conventional material, as expected, decreases the transmitted power of whole structure ( Figures 3.8(c), 3.8(d), 3.9(c) and 3.9(d) ). Fourth, while effect of loss in the bianisotropic slab decreases transmitted power around resonance frequencies  $f = 5 - 7 \text{ GHz}$  ( Figures 3.8(c) and 3.8(d) ), the effect of loss inside the conventional material (only is the dielectric loss considered since inclusion of the magnetic loss into the analysis does not change the conclusion drawn here) significantly decreases the sharp ripples in the reflected powers beyond resonance frequencies (Figures 3.8(a), 3.8(b), 3.9(a) and 3.9(b)).



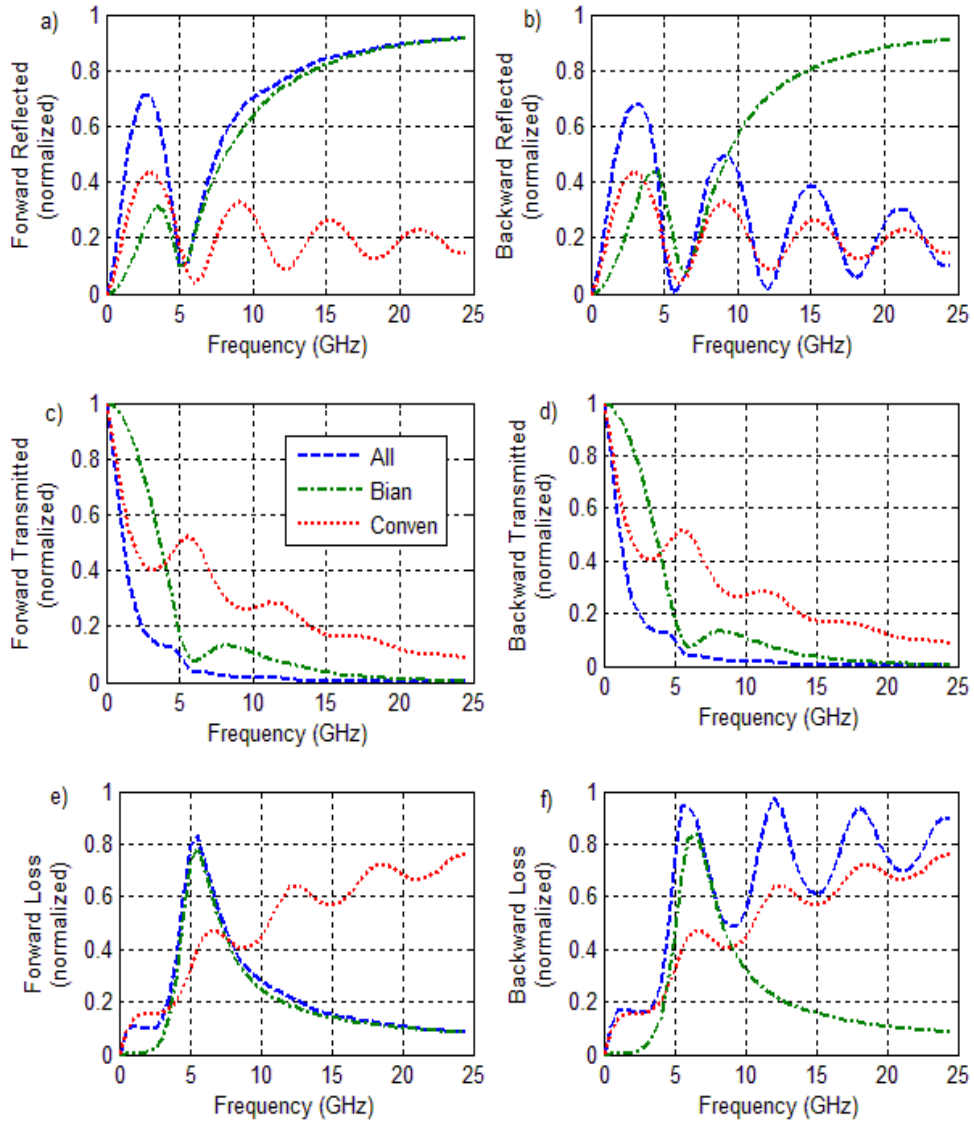


**Figure 3.7:** Dependencies of a) and b) reflected powers, c) and d) transmitted powers, e) and f) loss powers of the two-layer composite structure ( $L_1=L_2=10$ .mm ).

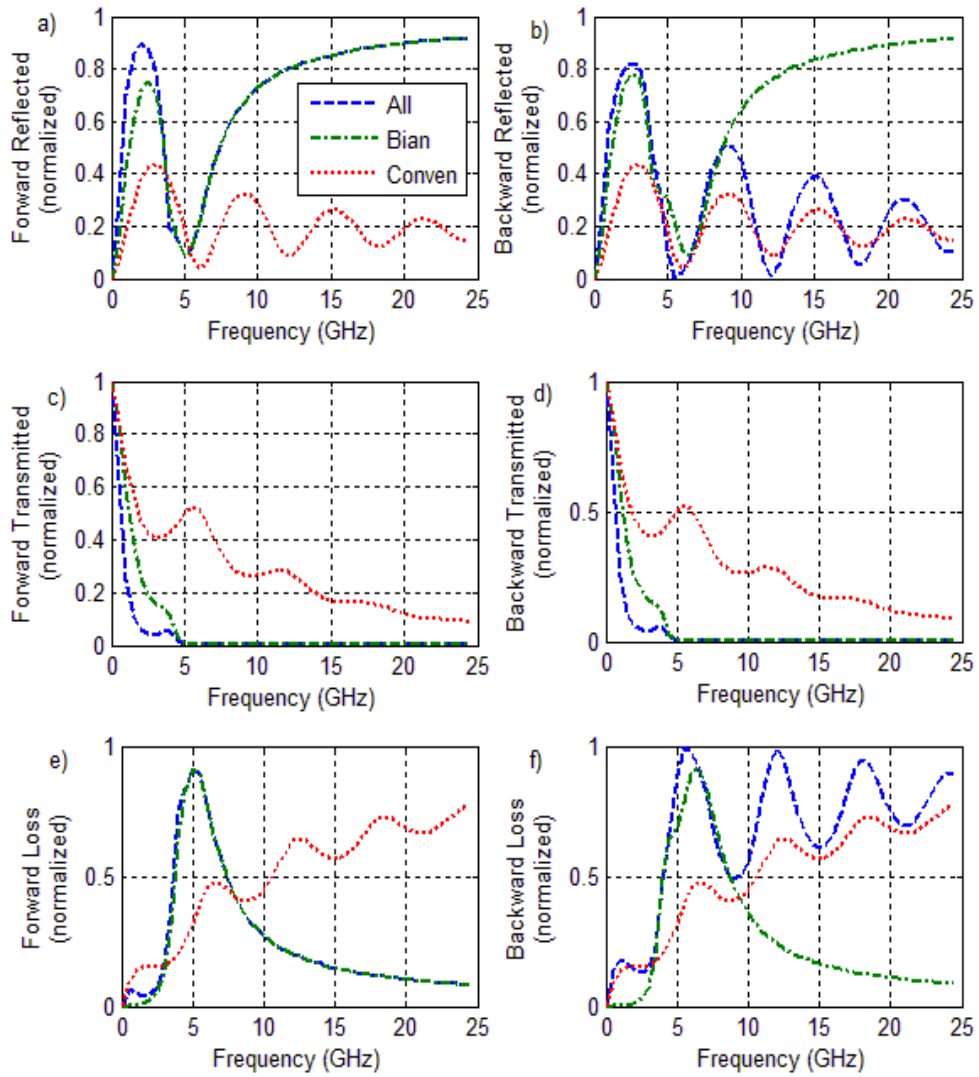


**Figure 3.8:** Dependencies of a) and b) reflected powers, c) and d) transmitted powers, e) and f) loss powers of the two-layer composite structure ( $L_1=40$ .mm,  $L_2=10$ .mm ).

## CHAPTER 4

### PROPAGATION CHARACTERISTICS OF A COMPOSITE MATERIAL BY SIMULATION PROGRAM CST

#### 4.1 Introduction

Up to this point, we analytically derived S - parameters in Chapter 2 and then also validated by a numerical analysis in Chapter 3. In this validation, we utilized the Lorentz dispersion model and some parameters without focusing the structure and size of the bianisotropic MM slab and the conventional material. In this chapter, we perform a simulation of the composite structure in Figure 3.1 by using split-ring resonators (SRRs).

Figure 4.1 shows a schematic of a commonly used edge coupled split ring resonator. The SRR structure consists of two concentric metallic rings that are both interrupted by a small gap. When a plane wave is incident in the x direction with an electrical field in the z direction and a magnetic field in the y direction, the SRR respond with a bianisotropic property. This is because the electrical field in the z direction can induce a magnetic dipole in the y direction due to the asymmetry of the inner and outer rings, while the magnetic field in the y direction can also induce an electrical dipole in the z direction [30].

Since the MM slab is bianisotropic, it produce different reflection properties. Therefore, forward and backward reflection and transmission S-parameter of the whole structure and the MM slab itself (and conventional material) are simulated separately to better analyze the simulation results.

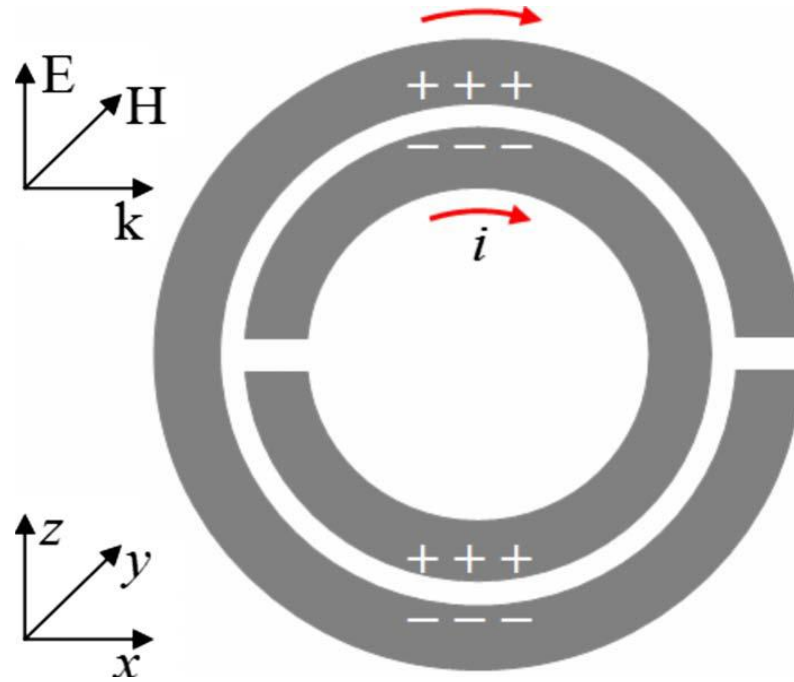


**Figure 4.1:** Schematic of a split-ring resonator used to construct metamaterials. When a plane wave polarized along the z-axis is incident in the x direction, the metamaterial will show bi-anisotropy [30].

#### 4.2 Analysis of the Isotropic Slab in CST

An isotropic material is one which looks the same in every direction. We can not define any special direction using the material properties. In other words, none of the properties depend the orientation; it is perfectly rotationally symmetric. Note that in order to be isotropic the material must be homogenous on the length scale of interest; i.e, the same at every point in the material. For instance, rubber is a very isotropic material. Take a rubber ball, and it will feel the same and bounce the same however you rotate it. On the other hand, wood is an anisotropic material: hit it with an axe and it will take more force to break of you are cutting across the grain than along it. We're thinking about the material rather than the shape of the object [54].

An isotropic medium is one such that the permittivity  $\epsilon$  and permeability  $\mu$  of the medium are uniform in all directions of the medium. When the isotropic material exposed to electrical field it demonstrates the right handed material properties. As in Figure 4.3 electric field is parallel to split in rings so that it behaves as a conventional material property [30].

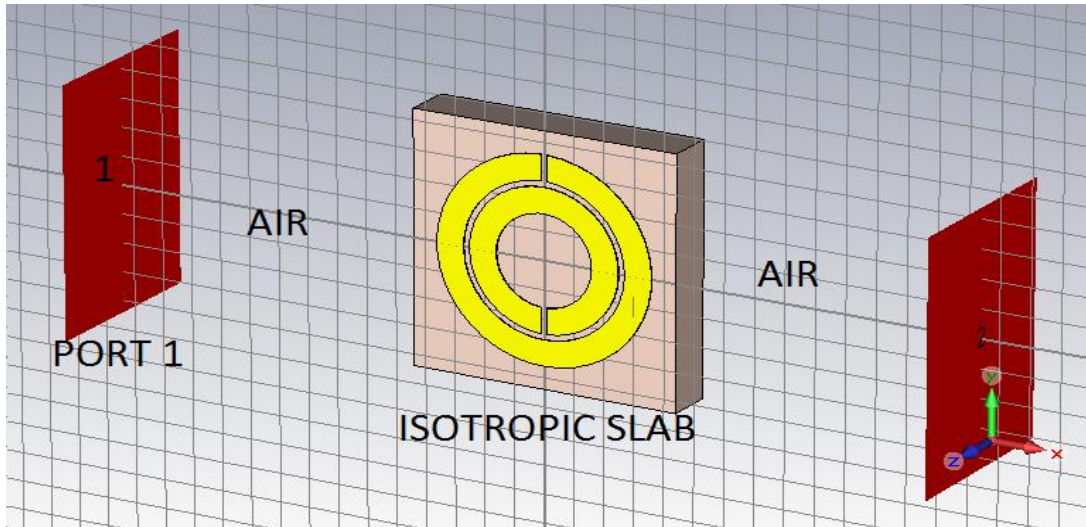


**Figure 4.2:** Simulation of isotropic slab in CST program

This in turn results in the same forward and backward reflection (and transmission) scattering parameters ( $S_{11} = S_{22}$  and  $S_{12} = S_{21}$ ).

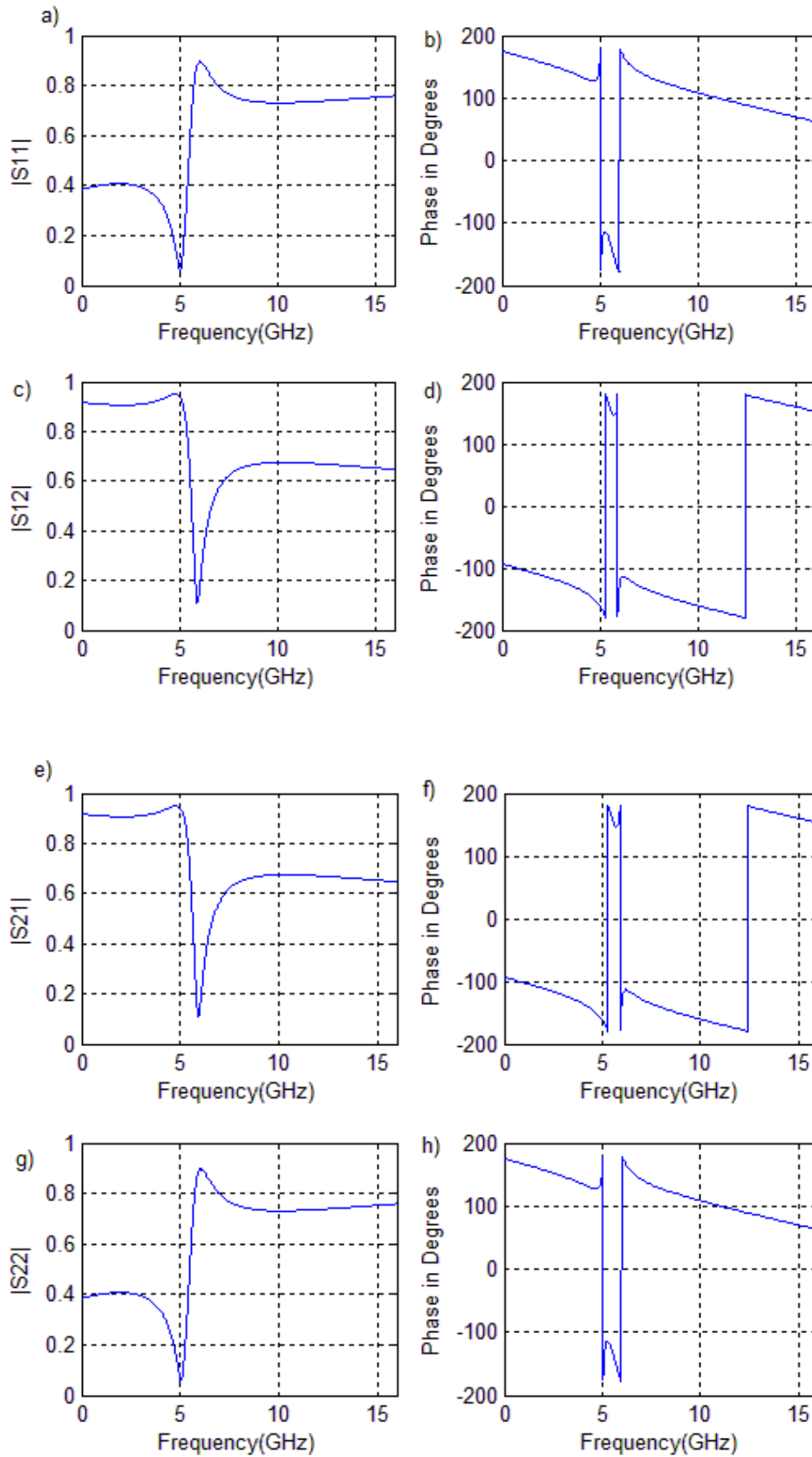


**Figure 4.3:** Magnitudes( (a), (c), (e), (g) ) and phases ((b), (d), (f), (h) ) of the forward(backward) transmission(reflection) constants of the isotropic slab.

### 4.3 Analysis of the Bianisotropic Slab in CST

Compared to an isotropic material, the most interesting and important feature of a bianisotropic material is that the characteristic impedances have different values for the waves propagating in the two opposite directions of the  $x$  axis [30]. As in Figure 4.5 splits of rings are rotated 90 degrees so that electric field is now perpendicular to the splits. Contrary to isotropic material bianisotropic metamaterial demonstrates the left handed property rules. The presentation of electric field is perpendicular to split on rings is shown in Figure 4.5. In our numerical validation of  $S$ - parameters in Chapter 3 we have resonance; however, energy cavity (resonance) also occurs here about 3 GHz.

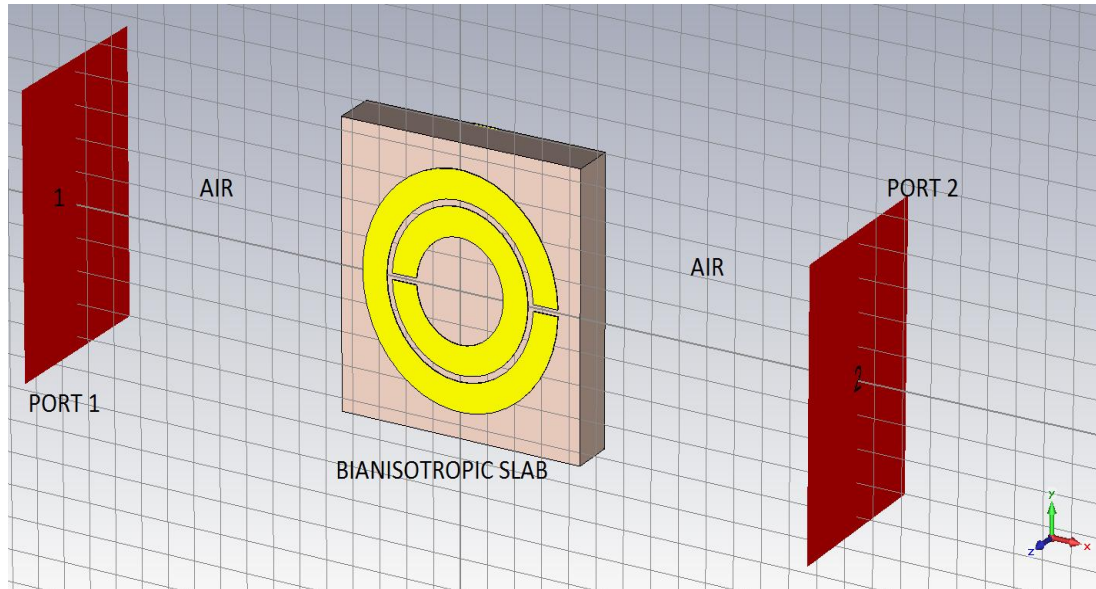


**Figure 4.4:** Simulation of bianisotropic slab in CST program

From the dependencies in Figure 4.5, we note that while forward and backward transmission scattering parameters ( $S_{21}$  and  $S_{12}$ ) are the same, forward and backward reflection scattering parameters ( $S_{11}$  and  $S_{22}$ ) are different, demonstrating the reflection asymmetric property of bianisotropic MM slabs.

We also notice from Figure 4.5 that the bianisotropic MM slab has a resonance behavior around 3 GHz, which can be seen from the sharp nulls of  $S_{11}$  and rapid change in  $S_{21}$ .

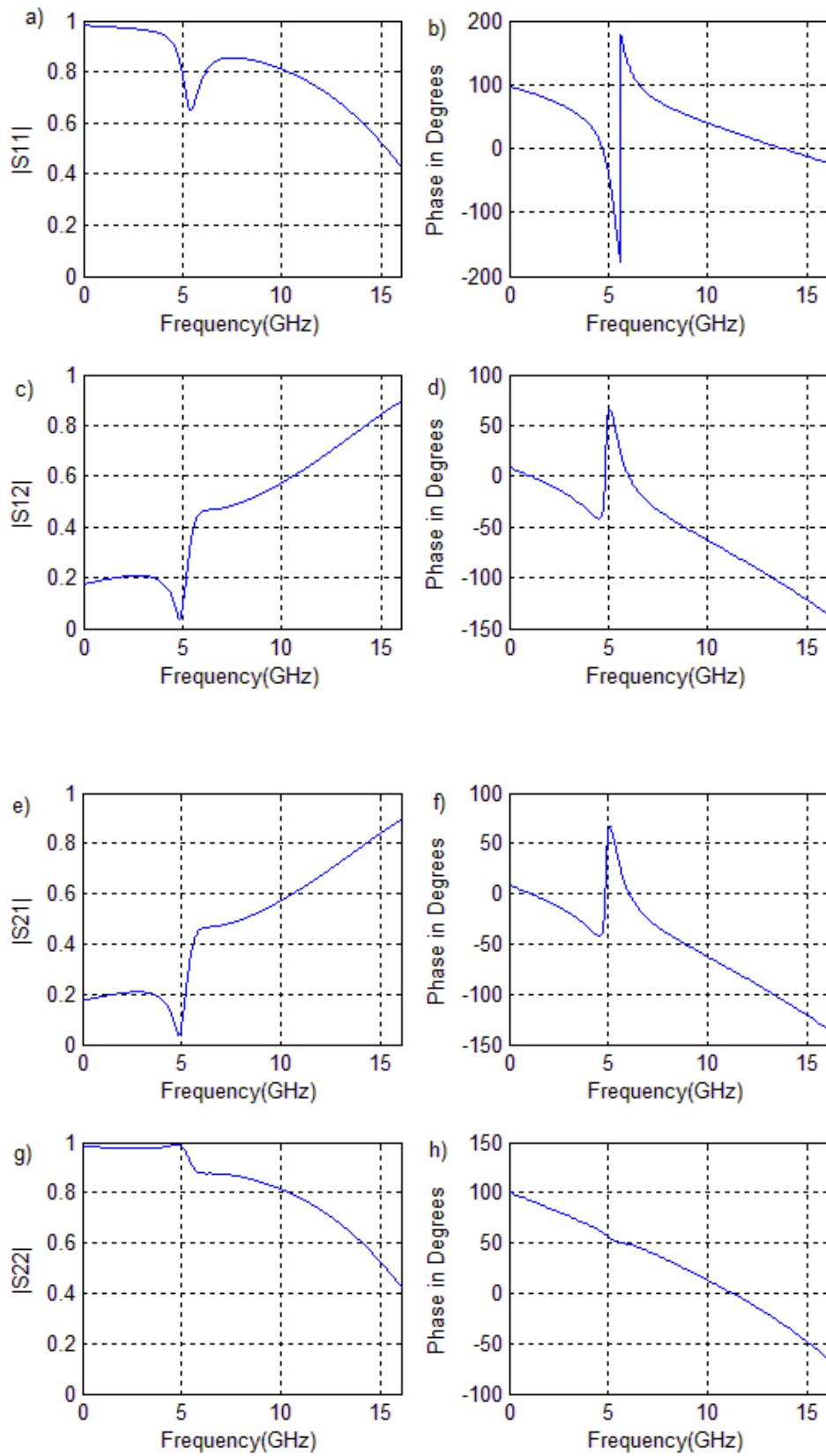


**Figure 4.5:** Magnitudes( (a), (c), (e), (g) ) and phases ((b), (d), (f), (h) ) of the forward(backward) transmission(reflection) constants of the bianisotropic slab.



#### 4.4 Analysis of Composite Structure in CST

The conventional material and bianisotropic metamaterial slab are combined respectively and applied into CST program as in Figure 4.7. When we analyze the result of the simulation in Figure 4.8, we see that there is resonance about 3 GHz as in bianisotropic metamaterial property in previous subsection. Moreover, the forward transmission ( $S_{21}$ ) and backward transmission ( $S_{12}$ ) constants are the same; however, forward reflection ( $S_{11}$ ) and backward reflection ( $S_{22}$ ) constant are different.

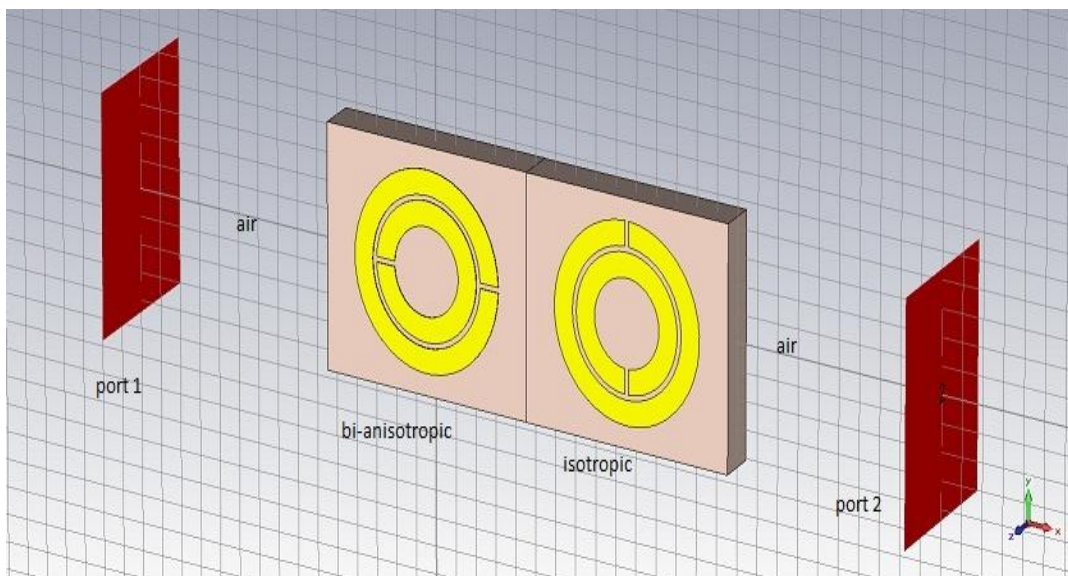


**Figure 4.6:** The problem under investigation in CST program

Therefore, we note that resonance behaviour of the composite structure is decided by the bianisotropic metamaterial with respect to isotropic material.

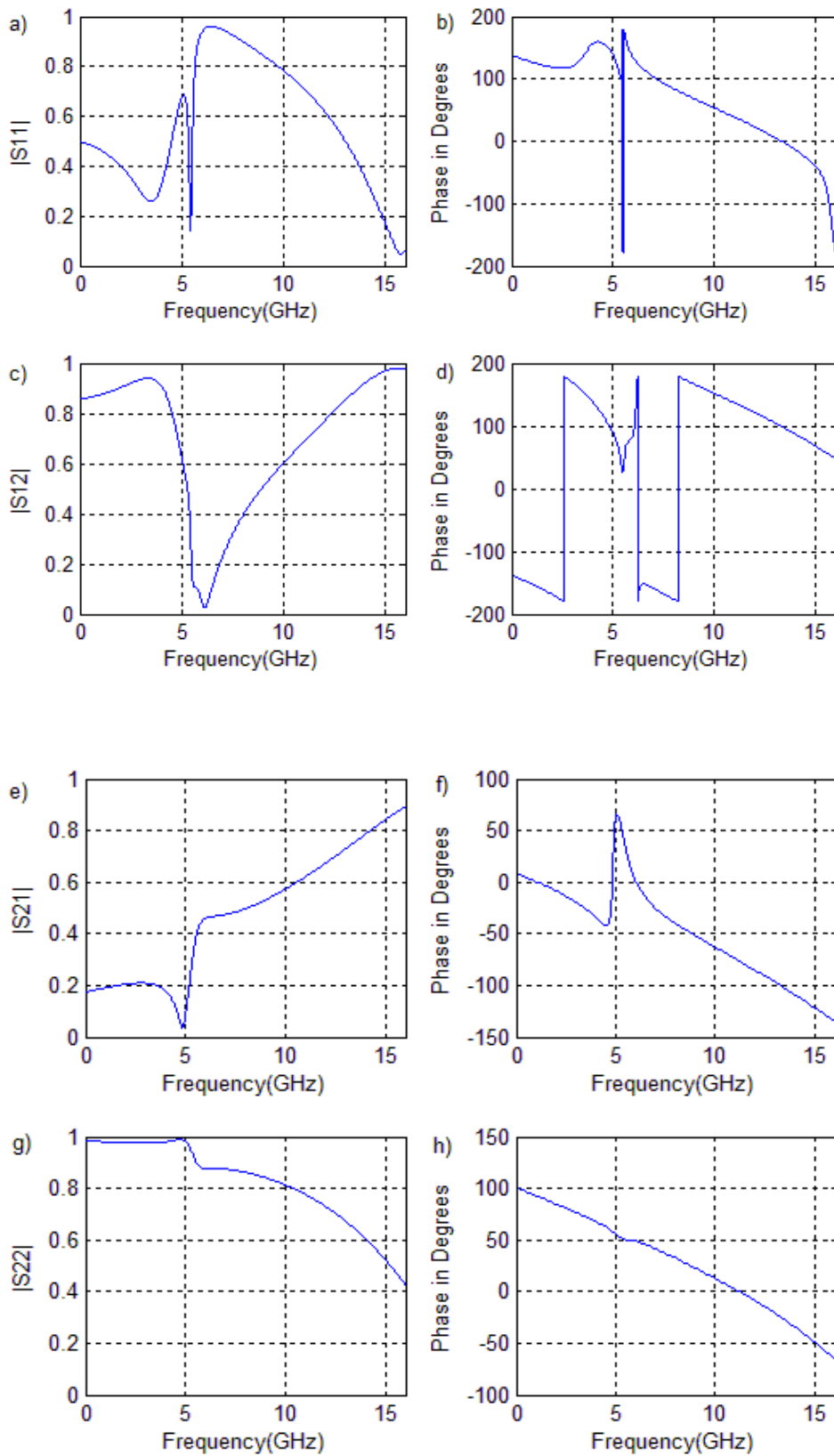


**Figure 4.7:** Magnitudes( (a), (c), (e), (g) ) and phases ((b), (d), (f), (h) ) of the forward(backward) transmission(reflection) constants of the composite structure.

## CHAPTER 5

### CONCLUSION

#### 5.1 Results

In this Master thesis, in first Chapter we presented how the metamaterial concept emerged, and then gave a brief literature review of isotropic and bi-anisotropic metamaterials. Then, we discussed the motivation of the thesis.

In the second Chapter, from the previous studies and using Maxwell equations we extracted electromagnetic bianisotropic metamaterial property parameters coupling coefficient ( $\xi_0$ ), relative complex permeability ( $\mu_{yy}$ ) and permittivity ( $\varepsilon_{zz}$ ) in terms of refractive-index. Towards this end, necessary scattering parameters of forward reflection ( $S_{11}$ ), backward transmission ( $S_{12}$ ), forward transmission ( $S_{21}$ ) and backward reflection ( $S_{22}$ ) coefficients are derived analytically utilizing boundary conditions for the investigated two-layer composite structure.

In addition, from the derived aforementioned constant parameters and boundary conditions, we derived complex power relations for a composite structure with a bianisotropic metamaterial slab and a conventional material. To the best knowledge of us, such derivation are new to the literature.

In Chapter 3, we turned our attention to validation of the derived expressions in the Chapter 2, and also we performed a numerical analysis to achieve our goal. In the analysis, we used Lorentz dispersion model to simulate artificial bi-anisotropic slab and the conventional material as well as to analyze the propagation characteristics of the composite material. In addition to this model we utilized the transfer matrix method,

which is an appropriate model for analysis of cascaded structures, to validate derived expressions.

In Chapter 4, we simulated a two-layer composite material structure (a bi-anisotropic MM slab and a conventional material) by using split ring resonators (SRRs) in a computer simulation program CST for comparisons of the results in Chapter 3.

From analytical model and simulation results, we note that the analyzed composite structure has different reflection scattering parameters and then different reflected powers, whereas it has the same transmission scattering parameters and the same transmitted powers. In addition, we note that bianisotropic metamaterials have different loss power behaviors depending on wave propagation direction.

From the dependencies given in Chapter 3, we note that resonance behaviour of the composite structure is managed by the bianisotropic metamaterial with respect to isotropic material

## **5.2 Future Work**

As a future work, we investigate composite structure composed of bianisotropic MM sandwiched between two left handed material. In addition, complex power analysis will be expanded in detail for realizing the exact transmission, reflection and loss powers.

## REFERENCES

- [1] Kock, W. E. (1946). Metal-Lens Antenna. *IRE Proc*, **34**, 828.
- [2] Veselago, V. G. (1968). The electrodynamics of substances with simultaneously negative values of  $\epsilon$  and  $\mu$ . *Sov. Phys. Usp*, **10**, 509–14.
- [3] Caloz, C., Chang, C., Itoh, T. (2001). Full-wave verification of the fundamental properties of left-handed materials in waveguide configurations. *J. Appl. Phys*, **90**, 11.
- [4] Eleftheriades, G.V., Iyer A.K., Kremer, P.C. (2002). Planar Negative Refractive Index Media Using Periodically L-C Loaded Transmission Lines. *IEEE Transactions on Microwave Theory and Techniques*, **50**, 2702–2712.
- [5] Caloz, C., Itoh, T. (2002). Application of the Transmission Line Theory of Left-handed (LH) Materials to the Realization of a Microstrip 'LH line'. *IEEE Antennas and Propagation Society International Symposium*, **2**, 412.
- [6] Pendry, J.B, Holden, A.J, Robbins, D.J, Stewart, W.J. (1998). Low Frequency Plasmons in Thin Wire Structures. *Condensed Matters*, **10**, 4785-4809.
- [7] Pendry, J.B, Holden, A.J, Robbins, D.J, Stewart, W.J. (1999). Magnetism from Conductors and Enhanced Nonlinear Phenomena. *IEEE Transactions on Microwave Theory and Techniques*. **47**, 2075-2084.
- [8] Engheta N, Richard W. Ziolkowski. (2006). *Metamaterials: Physics and Engineering Explorations*. USA : Wiley & Sons.
- [9] Zouhdi S, Ari S, Alexey P. Vinogradov. (2008). *Metamaterials and Plasmonics: Fundamentals, Modelling, Applications*. New York: Springer-Verlag.
- [10] Smith, David R. (2006). "What are Electromagnetic Metamaterials?". *Novel Electromagnetic Materials*. The research group of D.R. Smith. Retrieved 2009.
- [11] Shelby, R. A., Smith D.R., Shultz S. (2001). Experimental Verification of a Negative Index of Refraction. *Science*, **292**, 77–9.
- [12] Pendry, John B. (2004). Negative Refraction. *Contemporary Physics. Princeton University Press*, **45**, 191–202.

- [13] Guenneau, S., Alexander M., Gunnar P., Anantha, S. R. (2007). Acoustic metamaterials for sound focusing and confinement. *New Journal of Physics*. **9**, 1367–2630.
- [14] Brun, M., Guenneau, S. and Movchan, A. B. (2009). Achieving control of in-plane elastic waves. *Appl. Phys. Lett*, **94**, 1–7.
- [15] Smith, David R; Research group (2005). "Novel Electromagnetic Materials program". Retrieved 2009-08-17.
- [16] Rainsford, T. J., Samuel, M. P., Abbott, D. (2005). T-ray sensing applications review of global developments. *Proc. SPIE*, **17**, 826–838.
- [17] Cotton, Micheal G. (2003). Applied Electromagnetics. *2003 Technical Progress Report (NITA – ITS)* (Boulder, CO, USA: NITA – Institute for Telecommunication Sciences). Telecommunications Theory (3): 4–5. Retrieved 2009-09-14.
- [18] Alici, K. B., Özbay, E. (2007). Radiation properties of a split ring resonator and monopole composite. *Physica status solidi (b)*, **244**, 1192.
- [19] Hapgood, Fred; Grant, Andrew. (2010). Metamaterial Revolution: The New Science of Making Anything Disappear. **1**, 2-6.
- [20] McDonald, Kim. (2000). UCSD Physicists Develop a New Class of Composite Material with 'Reverse' Physical Properties Never Before Seen. UCSD Science and Engineering. Retrieved 2010-12-17.
- [21] Pendry, John B., Smith, David R. (2006). The Quest for the Superlens. *Scientific American*, **295**, 60.
- [22] R. A. Depine and A. Lakhtakia. (2004). A new condition to identify isotropic dielectric-magnetic materials displaying negative phase velocity. *Microwave and Optical Technology Letter*, **41**, 315-319.
- [23] Eleftheriades, G.V., Keith G.B. (2005). Negative-refraction metamaterials: fundamental principles and applications. Wiley: John & Sons.

- [24] Alu, A., Nader E. (2004). Guided Modes in a Waveguide Filled With a Pair of Single-Negative (SNG), Double-Negative (DNG), and/or Double-Positive (DPS) Layers. *IEEE Transactions on Microwave Theory and Techniques*, **52**, 199-200.
- [25] Marques, R., Medina, F., Rafii-El-Idrissi, R. (2002). Role of bianisotropy in negative permeability and left-handed metamaterials. *Physical Review B*, **65**, 144440–144454.
- [26] Rill, M. S. (2008). Negative-index bianisotropic photonic metamaterial fabricated by direct laser writing and silver shadow evaporation. *Optics Letter*, **34**, 19–21.
- [27] Kriegler, C. E. (2010). Bianisotropic photonic metamaterials. *IEEE journal of selected topics in quantum electronics*, **999**, 1–15.
- [28] Chen, X, Grzegorzcyk, T. M, Kong, J. A. (2006). Optimization Approach to the Retrieval of the Constitutive Parameters of a Slab of General Bianisotropic Medium. *Progress In Electromagnetics Research*, **60**, 1–18.
- [29] Hasar, U. C., Barroso, J. J. (2011). Retrieval approach for determination of forward and backward wave impedances of bianisotropic metamaterials. *Progress In Electromagnetics Research*, **112**, 109-124.
- [30] Li, Z., Aydin, K., Ozbay, E. (2009). Determination of the effective constitutive parameters of bianisotropic metamaterials from reflection and transmission coefficients. *Phys. Rev. E*. **79**, 26610-26617.
- [ 31] J. A. Kong, *Electromagnetic Wave Theory* (1990). Cambridge: Wiley.
- [32] Landau LD, Lifshitz EM. (1984). *Electrodynamics of continuous media*. Frankfurt: Pergamon Press.
- [33] Pendry J.B., Smith D.R. (2004). Reversing light with negative refraction. *Physics Today*, **57**, 37–43.
- [34] Chen, X., Wu, B.I., Kong, J. A., Grzegorzcyk, T. M. (2005). Retrieval of the effective constitutive parameters of bianisotropic metamaterials. *Phys. Rev. E*, **71**, 46610-46614.

- [35] Hasar, U. C., Barroso, J. J. (2011). Retrieval approach for determination of forward and backward wave impedances of bianisotropic metamaterials. *Progress In Electromagnetics Research*, **112**, 109–124.
- [36] Hasar, U. C., Bute, M., Barroso, J. J., Ertugrul, M. (2013). Unambiguous retrieval method for effective material parameters of homogeneous bianisotropic metamaterials. *Progress In Electromagnetics Research* (under revision).
- [37] Born M, Wolf E. (1964). Principles of optics: electromagnetic theory of propagation, interference and diffraction of light. Oxford: Pergamon Press.
- [38] Wikipedia. (2013). Transfer Matrix Method (TMM). [http://en.wikipedia.org/wiki/Transfer-matrix\\_method\\_\(optics\)](http://en.wikipedia.org/wiki/Transfer-matrix_method_(optics)), 25,08,2013.
- [39] Björk, G., Nelsson, O. (1987). A new exact and efficient numerical matrix theory of complicated laser structures; properties of asymmetric phase-shifted DFB lasers. *J.Lightwave Technol.*, **5**, 140 -146.
- [40] Born M, and Wolf E. (1965). Principles of Optics. 3rd edition. Oxford: Pergamon Press.
- [41] Hasar, U. C., Barroso, J. J., Sabah,C., Kaya,Y., Ertugrul, M. ( 2013). Stepwise technique for accurate and unique retrieval of electromagnetic properties of bianisotropic metamaterials. *J.Opt. Soc. Am. B*, **30**, 1058–1068.
- [42] Sabah, C. (2008). Effects of loss factor on plane wave propagation through a left-handed material slab. *Acta Phys. Pol. A*, **113**, 1589–1597.
- [43] Hasar, U. C., Ozbek, I. Y., Oral, E. A., Karacali, T., Efeoglu, H. (2012). The effect of loss silicon and fabrication tolerance on spectral properties of porous silicon Fabry-Perot cavities in sensing applications. *Opt. Express*, **20**, 2208–22223.
- [44] Hsieh, F. J., Wang, W. C. (2012). Full extraction methods to retrieve effective refractive index and parameters of a bianisotropic metamaterial based on material dispersion models. *J. Appl. Phys.*, **112**, 64907–64913.
- [45] Karacali, T., Hasar, U. C., Ozbek, I. Y., Oral, E. A., Efeoglu, H. (2013). Novel design of porous silicon based sensor for reliable and feasible chemical gas vapor detection. *J. Lightwave Technol.*, **31**, 295–305.



- [46] Hasar, U. C., Barroso, J. J., Sabah, C., Ozbek, I. Y., Kaya, Y., Dal, D., Aydin, T. (2012). Retrieval of effective electromagnetic parameters of isotropic metamaterials using reference-plane invariant expressions. *Progress in Electromagnetics Research*, **132**, 425–441.
- [47] Hasar, U. C. (2012). Reference-plane invariant, broadband, and stable constitutive parameters determination of low-loss materials from transmission-reflection measurements using variable parameters. *J. of Electromagnetic Waves and Appl.*, **26**, 44–53.
- [48] Humphrey, S. (2007). Direct calculation of the optical constants for a thin film using a midpoint envelope. *Applied Opt.*, **46**, 4660–4666.
- [49] Hasar, U. C. (2008). Two novel amplitude only methods for complex permittivity determination of medium- and low-loss materials. *Meas. Sci. Technol.*, **19**, 055706–055715.
- [50] Xu, S., Yang, L., Huang, L., Chen, H. (2011). Experimental measurement method to determine the permittivity of extra thin material using resonant metamaterials. *Progress In Electromagnetics Research*, **120**, 327–337.
- [51] Ekmekci, E., Sayan, G. T. (2013). Multi-functional metamaterial sensor based on a broad-side coupled SRR topology with a multi-layer substrate. *Appl. Phys. A*, **110**, 189–197.
- [52] Li, Z., Aydin, K., Ozbay, E. (2012). Retrieval of effective parameters for bianisotropic metamaterials with omega shaped metallic inclusions. *Photonics Nanostruct. Fundam. App*, **10**, 329–336.
- [53] Dong, Z., Lei, G.S.Y., Li, Q., Xu, M. X., Liu, H., Li, T., Wang, F. M. and Zhu, S. N.. (2007). Non-left-handed transmission and bianisotropic effect in a  $\pi$ -shaped metallic metamaterial. *Phys. Rev. B*, **75**, 075117-075123.
- [54] Wikipedia Answers. Math and Arithmetic, Wood Crafts. (2013). [http://wiki.answers.com/Q/What\\_is\\_isotropic\\_material\\_explain\\_with\\_example#page3](http://wiki.answers.com/Q/What_is_isotropic_material_explain_with_example#page3), 25.08.2013.

## APPENDIX

This is a Matlab program for, in addition to calculation of some derived expressions in Chapter 2, obtaining scattering parameters and power expressions in Chapter 3 (Figures 3.1-3.8) of this thesis.

```
clc;
clear all;
format long eng;
format compact;

Eps_zero = (10e-9)/(36*pi);
Mu_zero = 4*pi*1e-7;
c = 2.997925e8;
%
%----- We took time reference as exp(-iwt) -----
%
%      =====          Bianisotropic      MM      parameters
%      =====
F_e = 0.4;
F_m = 0.4;
F_Xi = 0.15;

f_e = 6e9;
f_m = 5e9;
f_Xi = 5e9;

Gamma_e = 2e9;
Gamma_m = 2e9;
Gamma_Xi = 2e9;

d1 = 10e-3;
%
=====

%      =====          Isotropic      MM      parameters
%      =====
Er1 = 6 + 1i*0.0;
%Er1=20;
Mr1 = 1 + 1i*0.0;

d2 = 10e-3;
%
=====

index = 0;
Z0 = sqrt(Mu_zero/Eps_zero);
% for f = 1e9: 50e7: 1e9,
for f = 0.1e1: 50e7: 25e9,
    index = index + 1;
    w = 2*pi*f;
```

```

k0 = (w/c);
k01=k0*Er1*Mr1;

% ===== Bianisotropic MM slab
=====
Eps_z_Values(index) = 1 - (F_e*f^2)/(f^2 - f_e^2 +
1i*Gamma_e*f);
Mu_y_Values(index) = 1 - (F_m*f^2)/(f^2 - f_m^2 + 1i*Gamma_m*f);
Xi_zero_Values(index) = 1 - (F_Xi*f^2)/(f^2 - f_Xi^2 +
1i*Gamma_Xi*f);
n_Plus_Values(index) = sqrt(
Eps_z_Values(index)*Mu_y_Values(index) - ( Xi_zero_Values(index)
).^2 );
n_Minus_Values(index) = - sqrt(
Eps_z_Values(index)*Mu_y_Values(index) - ( Xi_zero_Values(index)
).^2 );
if imag( n_Plus_Values(index) ) >= 0
    Signal_Values(index) = 1;
else
    Signal_Values(index) = -1;
end
n_bian = Signal_Values(index)*sqrt(
Eps_z_Values(index)*Mu_y_Values(index) - ( Xi_zero_Values(index)
).^2 );
z_Plus = Mu_y_Values(index)/( n_bian + 1i*Xi_zero_Values(index)
);
z_Minus = Mu_y_Values(index)/( n_bian - 1i*Xi_zero_Values(index)
);

gamma_x = 1i*k0*n_bian;
Gamma_1 = (z_Plus - 1)/(z_Plus + 1);
Gamma_2 = (z_Minus - 1)/(z_Minus + 1);

%%Scatering parameters below are taken from the paper of
stepwise technique
%%for accurate and unique retrieval of electromagnetic
properties of
%%bianisotropic metamaterials equation of 1&2.

T_Values(index) = exp( gamma_x*d1 );
S11(index) = Gamma_1*(1 - T_Values(index)^2)/( 1 -
Gamma_1*Gamma_2*( T_Values(index) )^2 );
S22(index) = Gamma_2*(1 - T_Values(index)^2)/( 1 -
Gamma_1*Gamma_2*( T_Values(index) )^2 );
S21(index) = ( (1 - Gamma_1*Gamma_2)*T_Values(index) )/( 1 -
Gamma_1*Gamma_2*( T_Values(index) )^2 );
S12(index) = ( (1 - Gamma_1*Gamma_2)*T_Values(index) )/( 1 -
Gamma_1*Gamma_2*( T_Values(index) )^2 );

%% %%%Assuming the Zs and Zl are equal to 1 where the
reference paper name is
%% Full Extraction Method to Retrieve Effective Refractive
Index and
%% Parameters of a Bianisotropic Metamaterial

```

```
%%% equation 5
```

```
A = ( (1 + S11(index))* (1 - S22(index)) + S21(index)*S12(index)
)/(2*S21(index));
A2 = ( (1 + Gamma_1)*(1 - Gamma_2) + ( (1 - Gamma_1*Gamma_2)^2
+ Gamma_2*(1 - Gamma_1^2) - Gamma_1*(1 - Gamma_2^2)
)*T_Values(index)^2 ...
- Gamma_1*Gamma_2*(1 - Gamma_1)*(1 +
Gamma_2)*T_Values(index)^4 )/( 2*(1 - Gamma_1*Gamma_2)*( 1 -
Gamma_1*Gamma_2*T_Values(index)^2 )*T_Values(index) );
```

```
B = ( (1 + S11(index))* (1 + S22(index) ) - S21(index)*S12(index)
)/(2*S21(index));
```

```
B2 = ( (1+ Gamma_1)*(1+Gamma_2) -
(Gamma_1*(1+Gamma_2^2)+Gamma_2*(1+Gamma_1^2)+4*Gamma_1*Gamma_2+(1-
Gamma_1*Gamma_2)^2)*T_Values(index)^2 ...
+Gamma_1*Gamma_2*(Gamma_1+1)*(Gamma_2+1)*T_Values(index)^4)/(
2*(1 - Gamma_1*Gamma_2)*( 1 - Gamma_1*Gamma_2*T_Values(index)^2
)*T_Values(index));
```

```
C = ( (1 - S11(index))* (1 - S22(index)) - S21(index)*S12(index)
)/(2*S21(index));
```

```
C2 = ( (1 - Gamma_1)*(1 - Gamma_2) + ( Gamma_2*(1 - Gamma_1)^2 +
Gamma_1*(1 - Gamma_2)^2 - (1 - Gamma_1*Gamma_2)^2
)*T_Values(index)^2 ...
+ Gamma_1*Gamma_2*(1 - Gamma_1)*(1 -
Gamma_2)*T_Values(index)^4 )/(2*(1-Gamma_1*Gamma_2)*(1-
Gamma_1*Gamma_2*T_Values(index)^2)*T_Values(index) );
```

```
D = ( (1 - S11(index))* (1 + S22(index)) + S21(index)*S12(index)
)/(2*S21(index));
```

```
D2 = ( (1- Gamma_1)*(1+Gamma_2)+(Gamma_1*(1+Gamma_1*Gamma_2) -
Gamma_2*(1+Gamma_1*Gamma_2)+(1-Gamma_1*Gamma_2)^2)*T_Values(index)^2
...
+Gamma_1*Gamma_2*(Gamma_1*Gamma_2+ Gamma_2-Gamma_1-
1)*T_Values(index)^4)/(2*(1-Gamma_1*Gamma_2)*(1-
Gamma_1*Gamma_2*T_Values(index)^2)*T_Values(index));
```

```
% A(index)*D(index) - B(index)*C(index); % yields one
```

```
M1 = [A B; C D];
```

```
% S11_1 = (A + B - C - D)/(A + B + C + D)
```

```
%
```

```
=====
```

```
%
```

```
===== Isotropic MM slab
```

```
n = sqrt( Mr1*Er1 );
```

```
z = sqrt( Mr1/Er1 );
```

```

M2 = [ cos(k0*n*d2)  -1i*z*sin(k0*n*d2);  -1i*sin(k0*n*d2)/z
cos(k0*n*d2)  ];

% =====composite matrix of two material
=====

MT = M1*M2;
S11_1 = ( MT(1,1) + MT(1,2) - MT(2,1) - MT(2,2) )/( MT(1,1) +
MT(1,2) + MT(2,1) + MT(2,2) ); %%%reflection from transfer matrix
S22_1 = ( -MT(1,1) + MT(1,2) - MT(2,1) + MT(2,2) )/( MT(1,1) +
MT(1,2) + MT(2,1) + MT(2,2) ); %%%reflection backward from transfer
matrix
S21_1 = 2 / ( MT(1,1) + MT(1,2) + MT(2,1) + MT(2,2) ); %%%
transmission from transfer matrix
S12_1 = S21_1;

Lambda_1 = exp( -2i*k0*n*(d1 + d2) )*(1 + z)/(1 - z);
Lambda_2 = ( Lambda_1*exp( 1i*k0*n*d1 ) + exp( -1i*k0*n*d1 ) ) /
( Lambda_1*exp( 1i*k0*n*d1 ) - exp( -1i*k0*n*d1 ) );
Lambda_3 = exp( 2i*k0*n_bian*d1 )*( Lambda_2*z/z_Plus - 1) / (
Lambda_2*z/z_Minus + 1);
Lambda_4 = (1 + Lambda_3)/( (1/z_Plus) - Lambda_3/z_Minus );
S11_2 = ( Lambda_4 - 1 )/( Lambda_4 + 1 );%% reflection from
thesis document

% Lambda_5 = exp( -2i*k0*n_bian*(d1 + d2) )*(1 +
Z0/z_Minus)/(Z0/z_Plus - 1);
%
% Lambda_6 = ( Lambda_5 + exp( -2i*k0*n_bian*(d1) ) ) / (z*( -
Lambda_5/z_Plus+ exp( -2i*k0*n_bian*d1/z_Minus ) ) );
%
% Lambda_7 = exp( -2i*k0*n*d1 )*( Lambda_6 - 1) / ( Lambda_6 +
1);
%
% Lambda_8 = (1 + Lambda_7)/( Z0 - Lambda_7*Z0 );
%
% S22 = ( Lambda_8 - 1 )/( Lambda_8 + 1 ); %%% reflection from
thesis document
Lambda_5 = z_Minus*(1 + z_Plus)/(1 - z_Minus)/z_Plus;

Lambda_6 = ( Lambda_5 + exp( 2i*k0*n_bian*d2 ) )
)/(z*Lambda_5/z_Minus - z/z_Plus* exp( 2i*k0*n_bian*d2 ) );

Lambda_7 = ( Lambda_6 + 1 )/( Lambda_6 - 1)*exp( 2i*k0*n*d2 );

Lambda_8 = z*( Lambda_7 + exp(2i*k0*n*(d1+d2) ))/(Lambda_7 -
exp(2i*k0*n*(d1+d2) ) );

Omega_1 = 0.5*(1 + z)*exp( 1i*k0*(d1 + d2) )*exp( -1i*k0*n*(d1 +
d2) );
Omega_2 = ( -z*exp( 1i*k0*(d1 + d2) ) + Omega_1*exp( 1i*k0*n*(d1
+ d2) ) )*exp( 1i*k0*n*(d1 + d2) );
Omega_3 = ( 1 / (1 + z_Minus/z_Plus) )*( Omega_1*(1 +
z_Minus/z)*exp( 1i*k0*n*d1 ) ...

```

```

+ Omega_2*(1 - z_Minus/z)*exp( -1i*k0*n*d1 ) ) * exp( -
1i*k0*n_bian*d1 );
Omega_4 = ( Omega_1*exp( 1i*k0*n*d1 ) + Omega_2*exp( -1i*k0*n*d1
) - Omega_3*exp( 1i*k0*n_bian*d1 ) ) * exp( 1i*k0*n_bian*d1 );

S21_2 = 2*exp( 1i*k0*(d1 + d2) ) / ( Omega_3*(1 + 1/z_Plus) +
Omega_4*( 1 - 1/z_Minus ) );%% transmission from thesis document
S12_2 = S21_2;

% Omega_5 = ( (1/z_Plus + 1)/(1/z_Plus + 1/z_Minus) ) * exp( -
1i*k0*(d1 + d2) ) * exp( +1i*k0*n_bian*(d1 + d2) );
%
% Omega_6 = ( (1/z_Minus - 1)/(1/z_Plus + 1/z_Minus) ) * exp( -
1i*k0*n*(d1 + d2) ) * exp( -1i*k0*n_bian*(d1 + d2) );
%
% Omega_7 = (Omega_5*exp( -1i*k0*n_bian*d2 ) + Omega_6*exp(
1i*k0*n_bian*d2 ) ) * ( Omega_5*( 1 + z/z_Minus ) + Omega_6*exp(
+2i*k0*n_bian*d2 ) ) * (1 - z/z_Plus) ) ...
% / ( 2*( Omega_5 + Omega_6*exp( +2i*k0*n_bian*d2 ) ) ) *
exp( +1i*k01*n*d2 ) ;
%
% Omega_8 = (Omega_5*exp( -1i*k0*n_bian*d2 ) + Omega_6*exp(
+1i*k0*n_bian*d2 ) ) * ( Omega_5*( 1 - z/z_Minus ) + Omega_6*exp(
+2i*k0*n_bian*d2 ) ) * (1 + z/z_Plus) ) ...
% / ( 2*( Omega_5 + Omega_6*exp( +2i*k0*n_bian*d2 ) ) ) *
exp( -1i*k01*n*d2 ) ;
%
%
% S12 = 2*exp( -1i*k0*(d1 + d2) ) / ( Omega_7*(1 - 1/z) +
Omega_8*(1 + 1/z) );

%
% Omega_5 = z_Minus*(1 + z_Plus)*exp( -1i*k0*n_bian*d1 ) / (
2*(z_Plus + z_Minus) );
% Omega_6 = z_Plus*(1 - z_Minus)*exp( +1i*k0*n_bian*d1 ) / (
2*(z_Plus + z_Minus) );
% S12 = 2 / ( (1 + 1/z)*[ (1 + z/z_Minus)*Omega_5 + (1 -
z/z_Plus)*Omega_6 ] * exp( -1i*k0*n*d2 ) + ...
% (1 - 1/z)*[ (1 - z/z_Minus)*Omega_5 + (1 +
z/z_Plus)*Omega_6 ] * exp( +1i*k0*n*d2 ) ); %% transmission backward
from thesis
%

Lambda_9 = ( (1 + 1/z_Plus)*exp( -1i*k0*n_bian*d1 ) + (1/z_Minus
- 1)*exp( +1i*k0*n_bian*d1 ) ) ...
/ ( (z/z_Minus)*(1 + 1/z_Plus)*exp( -1i*k0*n_bian*d1 ) -
(z/z_Plus)*(1/z_Minus - 1)*exp( +1i*k0*n_bian*d1 ) );
Lambda_10 = z * ( (Lambda_9 + 1) + (Lambda_9 - 1)*exp( +2i*k0*n*d2
) ) ...
/ ( (Lambda_9 + 1) - (Lambda_9 - 1)*exp( +2i*k0*n*d2 ) );

S22_2 = (Lambda_10 - 1) / (Lambda_10 + 1);
%%=====00000000
00000000=====
=====

S11_Iso(index) = ( M2(1,1) + M2(1,2) - M2(2,1) - M2(2,2) ) / (
M2(1,1) + M2(1,2) + M2(2,1) + M2(2,2) );

```

```

S21_Iso(index) = 2 / ( M2(1,1) + M2(1,2) + M2(2,1) + M2(2,2) );

S12_Iso(index) = 2 / ( M2(1,1) + M2(1,2) + M2(2,1) + M2(2,2) );
S22_Iso(index) = ( -M2(1,1) + M2(1,2) - M2(2,1) + M2(2,2) ) / (
M2(1,1) + M2(1,2) + M2(2,1) + M2(2,2) );

%=====FORWARD=====
Transmittivity_Bian(index) = abs(S21(index))^2;
Transmittivity_Iso(index) = abs(S21_Iso(index))^2;
Transmittivity_All(index) = abs( S21_1 )^2;%===P_transmitted

Reflectivity_Bian(index) = abs(S11(index))^2;
Reflectivity_Iso(index) = abs(S11_Iso(index))^2;
Reflectivity_All(index) = abs( S11_1 )^2;%===P_reflected

Loss_Bian(index) = 1 - ( Transmittivity_Bian(index) +
Reflectivity_Bian(index) );
Loss_Iso(index) = 1 - ( Transmittivity_Iso(index) +
Reflectivity_Iso(index) );
Loss_All(index) = 1 - ( Transmittivity_All(index) +
Reflectivity_All(index) );

%=====BACKWARD=====

Transmittivity_Bian_2(index) = abs(S12(index))^2;
Transmittivity_Iso_2(index) = abs(S12_Iso(index))^2;
Transmittivity_All_2(index) = abs( S12_1 )^2;%===P_transmitted

Reflectivity_Bian_2(index) = abs(S22(index))^2;
Reflectivity_Iso_2(index) = abs(S22_Iso(index))^2;
Reflectivity_All_2(index) = abs( S22_1 )^2;%===P_reflected

Loss_Bian_2(index) = 1 - ( Transmittivity_Bian_2(index) +
Reflectivity_Bian_2(index) );
Loss_Iso_2(index) = 1 - ( Transmittivity_Iso_2(index) +
Reflectivity_Iso_2(index) );
Loss_All_2(index) = 1 - ( Transmittivity_All_2(index) +
Reflectivity_All_2(index) );

%=====

S21_1_real(index) = abs( S21_1 )^2
S21_1_imaginal(index) = imag( S21_1 )^2
S21_2_real(index) = abs( S21_1 )^2
S21_2_imaginal(index) = imag( S21_1 )^2

S12_1_real(index) = abs( S12_1 )^2
S12_1_imaginal(index) = imag( S12_1 )^2
S12_2_real(index) = abs( S12_1 )^2
S12_2_imaginal(index) = imag( S12_1 )^2

S11_1_real(index) = abs( S11_1 )^2
S11_1_imaginal(index) = imag( S11_1 )^2
S11_2_real(index) = abs( S11_1 )^2
S11_2_imaginal(index) = imag( S11_1 )^2

S22_1_real(index) = abs( S22_1 )^2
S22_1_imaginal(index) = imag( S22_1 )^2

```

```

S22_2_real(index) = abs( S22_1 )^2
S22_2_imaginal(index) = imag( S22_1 )^2

f_Values(index) = f/1e9;

end

%
PARAMETER=====S-

%=====s11

subplot(2,2,1)
plot(f_Values,S11_1_real,'b-' );
ylabel('|S11|');
xlabel({'frequency (GHz)', ' '});
title('Numeric - TMM');
grid on;

subplot(2,2,2);
plot(f_Values, (180/pi)*atan2(S11_1_imaginal,S11_1_real),'b-' );
ylabel('degrees');
xlabel({'frequency (GHz)', ' '});
title('Numeric - TMM');
grid on;

subplot(2,2,3);
plot(f_Values,S11_2_real,'b-' );
xlabel('frequency (GHz)');
ylabel('|S11|');
title('Analytic');
grid on;
subplot(2,2,4);
plot(f_Values, (180/pi)*atan2(S11_2_imaginal,S11_2_real),'b-' );
xlabel('frequency (GHz)');
ylabel('degrees');
title('Analytic');
grid on;

figure;

%=====s21

subplot(2,2,1)
plot(f_Values,S21_1_real,'b-' );
ylabel('|S21|');
xlabel({'frequency (GHz)', ' '});
title('Numeric - TMM');
grid on;

subplot(2,2,2);
plot(f_Values, (180/pi)*atan2(S21_1_imaginal,S21_1_real));
ylabel('degrees');
xlabel({'frequency (GHz)', ' '});
title('Numeric - TMM');
grid on;

```



```

subplot(2,2,3);
plot(f_Values,S21_2_real);
xlabel('frequency (GHz)');
ylabel('|S21|');
title('Analytic');
grid on;
subplot(2,2,4);
plot(f_Values,(180/pi)*atan2(S21_2_imaginal,S21_2_real));
xlabel('frequency (GHz)');
ylabel('degrees');
title('Analytic');
grid on;
figure;
%=====s12
subplot(2,2,1)
plot(f_Values,S12_1_real,'b-' );
ylabel('|S12|');
xlabel({'frequency (GHz)', ' '});
title('Numeric - TMM');
grid on;

subplot(2,2,2);
plot(f_Values,(180/pi)*atan2(S12_1_imaginal,S12_1_real));
ylabel('degrees');
xlabel({'frequency (GHz)', ' '});
title('Numeric - TMM');
grid on;

subplot(2,2,3);
plot(f_Values,S12_2_real);
xlabel('frequency (GHz)');
ylabel('|S12|');
title('Analytic');
grid on;
subplot(2,2,4);
plot(f_Values,(180/pi)*atan2(S12_2_imaginal,S12_2_real));
xlabel('frequency (GHz)');
ylabel('degrees');
title('Analytic');
grid on;
figure;
%=====s22
subplot(2,2,1)
plot(f_Values,S22_1_real,'b-' );
ylabel('|S22|');
xlabel({'frequency (GHz)', ' '});
title('Numeric - TMM');
grid on;

subplot(2,2,2);
plot(f_Values,(180/pi)*atan2(S22_1_imaginal,S22_1_real));
ylabel('degrees');
xlabel({'frequency (GHz)', ' '});
title('Numeric - TMM');
grid on;

subplot(2,2,3);
plot(f_Values,S22_2_real);
xlabel('frequency (GHz)');
ylabel('|S22|');
title('Analytic');

```

```

grid on;
subplot(2,2,4);
plot(f_Values, (180/pi)*atan2(S22_2_imaginal,S22_2_real));
xlabel('frequency (GHz)');
ylabel('degrees');
title('Analytic');
grid on;

%%=====complex power
verification=====

E1_arti=1;
E1_eksi = S11_2*E1_arti;
E2_arti = E1_arti*(1+S11_2)/(1+Lambda_3);
E2_eksi = Lambda_3*E2_arti;

E3_eksi=E2_arti*(Lambda_3*exp(-1i*k0*n_bian*d1)+exp(1i*k0*n_bian*d1)
)/(Lambda_1*exp(1i*k0*n*d1)+exp(-1i*k0*n*d1));
E3_arti=E3_eksi*Lambda_1;

E4_arti=S21_2*E1_arti;

% P1 = ( 1/(2*Z0) )*( ( abs(E2_eksi)^2 )/conj( z_Minus ) - (
abs(E2_arti)^2 )/conj( z_Plus ) ...
% + ( conj( E2_eksi)*E2_arti )/conj( z_Minus ) - ( conj(
E2_arti)*E2_eksi )/conj( z_Plus ) );

% P1 = ( 1/(2*Z0) )*( abs( E1_eksi )^2 - abs(E1_arti)^2 -
conj(E1_eksi)*E1_arti - E1_eksi*conj( E1_arti ) );

p1_0 = (-0.5/Z0)*(
abs(E1_arti)^2+abs(E1_eksi)^2+E1_arti*conj(E1_eksi)-
E1_eksi*conj(E1_arti));
%P1_0 = (-0.5/Z0)*abs(E1_arti)^2*( abs(S11_1)^2+conj(S11_1)-S11_1 -
1 )

p2_0 = (-0.5/Z0)*(
abs(E2_arti)^2/conj(z_Plus)+abs(E2_eksi)^2/conj(z_Minus)...
+E2_arti*conj(E2_eksi)/conj(z_Minus)-
E2_eksi*conj(E2_arti)/conj(z_Plus));

% P1_01 = (-0.5)*abs(E1_arti)^2*abs(S21(index))^2*(1/conj(z_Plus));

% P1_01 = 1/(2*Z0)*abs(E1_arti)^2*4*z_Plus/abs(z_Plus+Z0)^2;

% p2_d1 = (-0.5/Z0)*( -abs(E2_arti)^2/conj(z_Plus) +
abs(E2_eksi)^2/conj(z_Minus)...
% + E2_arti*conj(E2_eksi)*exp(2i*k0*n_bian*d1)/conj(z_Minus) -
E2_eksi*conj(E2_arti)*exp(-2i*k0*n_bian*d1)/conj(z_Plus))

```

```

p2_d1 = (-0.5/Z0)*( - ( abs(E2_arti)^2 ) *exp( -2*k0*imag(n_bian)*d1
)/conj(z_Plus) + ( abs(E2_eksi)^2 ) *exp( +2*k0*imag(n_bian)*d1
)/conj(z_Minus)...
+ E2_arti*conj(E2_eksi)*exp( 2i*k0*real(n_bian)*d1
)/conj(z_Minus) - E2_eksi*conj(E2_arti)*exp( -2i*k0*real(n_bian)*d1
)/conj(z_Plus));

p3_d1 = (-0.5/conj(z*Z0))*( abs(E3_eksi)^2*exp(2*k0*imag(n)*d1) -
abs(E3_arti)^2*exp(-2*k0*imag(n)*d1) +
E3_arti*conj(E3_eksi)*exp(+2i*k0*real(n)*d1) ...
- E3_eksi*conj(E3_arti)*exp(-2i*k0*real(n)*d1) );

p3_d2 = (-0.5/conj(z*Z0))*( abs(E3_eksi)^2*exp(2*k0*imag(n)*(d1+d2))
- abs(E3_arti)^2*exp(-2*k0*imag(n)*(d1+d2)) +
E3_arti*conj(E3_eksi)*exp(+2i*k0*real(n)*(d1+d2)) ...
- E3_eksi*conj(E3_arti)*exp(-2i*k0*real(n)*(d1+d2)) );

p4_d2 = (0.5/Z0)*(abs(E4_arti)^2);

%%=====

%%%%%%%%%%%%

subplot(3,2,1);
plot(f_Values, Reflectivity_All,'--', f_Values, Reflectivity_Bian,'-
.', f_Values, Reflectivity_Iso,':', 'LineWidth', 1.5);
ylabel({'Forward Reflected','(normalized)'});
% xlabel({'frequency (GHz)'; ' c) ' ;' '});
xlabel('Frequency (GHz)');
ylim([0,1]);
grid on;

subplot(3,2,2);

plot(f_Values, Reflectivity_All_2,'--', f_Values,
Reflectivity_Bian_2,'-.', f_Values, Reflectivity_Iso_2,':',
'LineWidth', 1.5);
ylabel({'Backward Reflected','(normalized)'});
% xlabel({'frequency (GHz)'; ' d) ' ;' '});
xlabel('Frequency (GHz)');
ylim([0,1]);
grid on;

%%%%%%%%%%%%

subplot(3,2,3);
plot(f_Values, Transmittivity_All,'--', f_Values,
Transmittivity_Bian,'-.', f_Values,
Transmittivity_Iso,':', 'LineWidth', 1.5);
ylabel({'Forward Transmitted','(normalized)'});
% xlabel({'frequency (GHz)'; ' a) ' ;' '});
xlabel('Frequency (GHz)');

```

```

ylim([0,1]);
grid on;

subplot(3,2,4);

plot(f_Values,      Transmittivity_All_2,'--',      f_Values,
Transmittivity_Bian_2,'-.',      f_Values,
Transmittivity_Iso_2,':','LineWidth', 1.5);
ylabel({'Backward Transmitted','(normalized)'});
% xlabel({'frequency (GHz)'; ' b) ' ;' '});
xlabel('Frequency (GHz)');
ylim([0,1]);
grid on;

%%%%%%%%%%
subplot(3,2,5);

plot(f_Values, Loss_All,'--', f_Values, Loss_Bian,'-.', f_Values,
Loss_Iso,':','LineWidth', 1.5);
ylabel({'Forward Loss','(normalized)'});
% xlabel({'frequency (GHz)'; ' e) ' ;' '});
xlabel('Frequency (GHz)');
ylim([0,1]);
grid on;

subplot(3,2,6);
plot(f_Values,      Loss_All_2,'--',      f_Values,      Loss_Bian_2,'-.',
f_Values, Loss_Iso_2,':','LineWidth', 1.5);
ylabel({'Backward Loss','(normalized)'});
% xlabel({'frequency (GHz)'; ' f) ' ;' '});
xlabel('Frequency (GHz)');
ylim([0,1]);
grid on;
%%

%=====TRANSMITTANCE=====
%=====
figure;
% plot(f_Values,      Transmittivity_All,      'b-','x'      ,      f_Values,
Transmittivity_Bian,      'r-','o',      f_Values,      Transmittivity_Iso,      'g-
','k');
subplot(2,2,1);
plot(f_Values,Transmittivity_All,'b-' );
% text(f_Values,Transmittivity_All,'o' );
title('TOTAL TRANSMISSION ');
xlabel({'frequency (GHz)'; ' a) ' ;' '});

ylabel('TRANSMITTANCE');
grid on;
% figure,
subplot(2,2,2);

plot(f_Values,Transmittivity_Bian,'r-' );
% text(f_Values,Transmittivity_All,'*' );
title('TRANSMISSION OF BI-ANISOTROPIC SLAB ');
xlabel({'frequency (GHz)'; ' b) ' ;' ' });
ylabel('TRANSMITTANCE');

```

```

grid on;
% figure,

subplot(2,2,3);
plot(f_Values,Transmittivity_Iso,'g-' );
%text(f_Values,Transmittivity_All,'+' );
title('TRANSMISSION OF ISOTROPIC SLAB');
xlabel({'frequency (GHz)'; ' c ' ;' '});
ylabel('TRANSMITTANCE');
grid on;
% figure,

subplot(2,2,4);

%          plot(f_Values,      Transmittivity_All,'b-',      f_Values,
Transmittivity_Bian,'r-', f_Values, Transmittivity_Iso,'g-');
plot(f_Values,      Transmittivity_All,'b-',      f_Values,
Transmittivity_Bian,'r-', f_Values, Transmittivity_Iso,'g-');
% text(f_Values, Transmittivity_All,'x');
% text(f_Values, Transmittivity_Bian,'*');
% text(f_Values, Transmittivity_Iso,'+');
title('ALL TRANSMISSION ');
xlabel({'frequency (GHz)'; ' d ' ;' ' });
ylabel('TRANSMITTANCE');

text(6,0.8,'Isotropic');
text(9,0.2,'Bianisotropic');
text(1.5,0.2,'Total');

grid on;

%

%%%=====REFLECTANCE=====
=====
figure;
%      plot(f_Values,      Reflectivity_All,      'b-',      f_Values,
Reflectivity_Bian, 'r-', f_Values, Reflectivity_Iso, 'g-');
subplot(2,2,1);
plot(f_Values,Reflectivity_All,'b-' );
% text(f_Values,Reflectivity_All,'x' );
title('TOTAL REFLECTION ');
xlabel({'frequency (GHz)'; ' a ' ;' '});
ylabel('REFLECTANCE');
grid on;
% figure,
subplot(2,2,2);

plot(f_Values,Reflectivity_Bian,'r-' );
% text(f_Values,Reflectivity_Bian,'*' );
title('REFLECTION OF BI-ANISOTROPIC SLAB');
xlabel({'frequency (GHz)'; ' b ' ;' '});
ylabel('REFLECTANCE');
grid on;
% figure,
subplot(2,2,3);

plot(f_Values,Reflectivity_Iso,'g-' );

```

```

% text(f_Values,Reflectivity_Iso,'+' );
title('REFLECTION OF ISOTROPIC SLAB');
xlabel({'frequency (GHz)'; ' c) ' ;' '});
ylabel('REFLECTANCE');
grid on;
% figure,

subplot(2,2,4);

plot(f_Values, Reflectivity_All,'b-', f_Values, Reflectivity_Bian,'r-', f_Values, Reflectivity_Iso,'g-');
% text(f_Values, Reflectivity_All,'x');
% text(f_Values, Reflectivity_Bian,'*');
% text(f_Values, Reflectivity_Iso,'+');
title('ALL REFLECTION ');
xlabel({'frequency (GHz)'; ' d) ' ;' '});
ylabel('REFLECTANCE');

text(15,0.4,'Isotropic');
text(9,0.75,'Bianisotropic');
text(3,0.8,'Total');

grid on;
%

%
=====LOSS=====
=====
figure;
% plot(f_Values, Loss_All, 'b-', f_Values, Loss_Bian, 'r-',
f_Values, Loss_Iso, 'g-');
% grid on;

subplot(2,2,1);
plot(f_Values,Loss_All,'b-' );
% text(f_Values,Loss_All,'x' );
title('TOTAL LOSS ');
xlabel({'frequency (GHz)'; ' a) ' ;' '});
ylabel('LOSS');
grid on;
% figure,
subplot(2,2,2);

plot(f_Values,Loss_Bian,'r-' );
% text(f_Values,Loss_Bian,'*' );
title('LOSS OF BI-ANISOTROPIC MEDIUM ');
xlabel({'frequency (GHz)'; ' b) ' ;' '});
ylabel('LOSS');
grid on;
% figure,
subplot(2,2,3);

plot(f_Values,Loss_Iso,'g-' );
% text(f_Values,Loss_Iso,'+' );
title('LOSS OF ISOTROPIC MEDIUM');
xlabel({'frequency (GHz)'; ' c) ' ;' '});
ylabel('LOSS');
grid on;
% figure,

```

```

subplot(2,2,4);

plot(f_Values, Loss_All,'b-', f_Values, Loss_Bian,'r-', f_Values,
Loss_Iso,'g-');
% text(f_Values, Loss_All,'x');
% text(f_Values, Loss_Bian,'*');
% text(f_Values, Loss_Iso,'+');
title('ALL LOSS ');
xlabel({'frequency (GHz)'; ' d) ' ;' '});
ylabel('LOSS');

% text(18,0.54,'Isotropic(+)');
% text(12,0.1,'Bianisotropic(*)');
% text(3,0.75,'All(x)');

grid on;

=====FINISH=====

```

# Electromagnetic Properties of Various $\pi$ -Shaped Bi-anisotropic Composite Metamaterials

Musa Bute and Ugur C Hasar

University of Gaziantep

Department of Electrical and Electronics Engineering

Gaziantep, 27310, Turkey

mbute@gantep.edu.tr and uhasar@gantep.edu.tr

**Özet:** Among various bi-anisotropic metamaterial (MM) slabs,  $\pi$ -shaped ones can allow miscellaneous configurations so that different and exciting electromagnetic properties of bi-anisotropic MM slabs can be readily achieved. We investigate the constitutive parameters of various  $\pi$ -shaped bi-anisotropic composite MM such as, refractive index ( $n$ ), permittivity ( $\epsilon$ ), permeability ( $\mu$ ) and magneto-electric coupling coefficient ( $\xi$ ). To achieve this purpose we mainly focus on the change in the width of continuous wire constituent and width of separated continuous wire of Composite bi-anisotropic MM and supported by simulations, the microwave studio package of CST simulation program has been used after obtaining the S-parameters.

## 1. Introduction

Artificially fabricated metamaterials (MMs) have drawn considerable attention of scientific community since they possess negative refractive index ( $n$ ) and negative refraction at a certain frequency band or bands [1]. Bi-anisotropic metamaterials can possess a coupling factor and surprisingly can have a backward wave medium property although their real part of  $n$  is not negative. Among various bi-anisotropic MM slabs,  $\pi$ -shaped ones can allow miscellaneous configurations so that different and exciting electromagnetic properties of bi-anisotropic MM slabs can be readily achieved. Because various electromagnetic devices can be produced with miscellaneous MM configurations, their compatibility should be investigated. To achieve this goal, electromagnetic properties of MM structures should be properly defined and retrieved. In this study, we investigate the influence of a change in the width ( $w_1$ ) of continuous wire constituent and width ( $w_2$ ) of separated continuous wire of various Composite bi-anisotropic MM slabs (combination of imparted continuous wire and  $\pi$ -shaped structure) on their electromagnetic parameters. Fig. 1 demonstrates the analyzed Composite slab with dimensions. It is assumed that the slab is periodic over  $y$ - $z$  plane. For the geometry and wave configuration, only  $\epsilon_y$ ,  $\mu_z$ , and  $\xi_0$  describe wave behavior among other constitutive parameters.



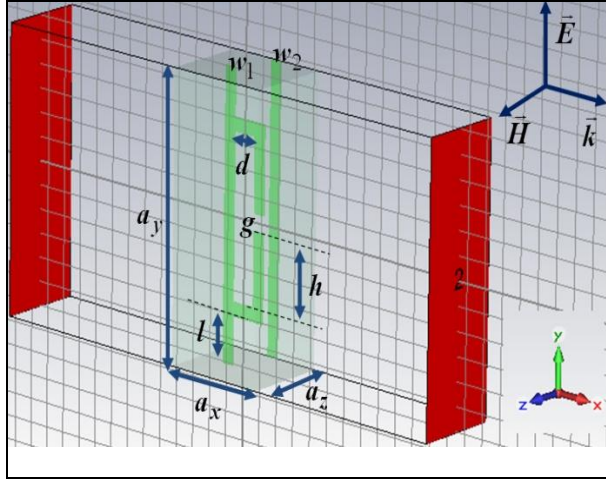


Fig. 1. Geometrical configuration of the analyzed Composite MM slab in addition to wave configuration.

## 2. Theoretical Background

To perform aforementioned quantitative analyses the phase unwrapping technique can be applied for unique and correct retrieval of electromagnetic properties of  $\pi$ -shaped bi-anisotropic MM slabs. This technique was applied for unique extraction of electromagnetic properties of isotropic conventional and MM samples [2,3]. Assuming that a uniform plane wave with polarization in the  $+y$  direction and propagation in  $+x$  direction is incident to both MM configuration in Fig. 1, forward and backward reflection and transmission S-parameters of each configuration with length  $L$  can be written for  $\exp(-i\omega t)$  time reference as

$$S_{11} = \frac{\Gamma_1(1-T^2)}{1-\Gamma_1\Gamma_2T^2}, \quad S_{22} = \frac{\Gamma_2(1-T^2)}{1-\Gamma_1\Gamma_2T^2}, \quad S_{21} = S_{12} = \frac{(1-\Gamma_1\Gamma_2)T}{1-\Gamma_1\Gamma_2T^2} \quad (1.1)$$

$$\Gamma_{(1,2)} = \frac{z_w^{+(-)} - 1}{z_w^{+(-)} + 1}, \quad z_w^+ = \frac{\mu_z}{n \mp i\xi_0}, \quad T = e^{ik_0nL}, \quad n = \mp \sqrt{\varepsilon_y\mu_z - \xi_0^2}. \quad (1.2)$$

Here,  $\Gamma_1$  and  $\Gamma_2$  are the intrinsic (first) reflection coefficients at the interfaces of front and back faces of each MM slab;  $T$  is the propagation factor related to propagation characteristics of the slabs;  $z_w^+$ ,  $z_w^-$ ,  $n$ , and  $k_0$  are, respectively, the normalized wave impedances in forward ( $+x$ ) and backward ( $-x$ ) directions, the refractive index of each bi-anisotropic MM slab, and the free-space wave number;  $\varepsilon_y$  is the relative complex permittivity in  $y$  direction;  $\mu_z$  is the relative complex permeability in  $z$  direction; and  $\xi_0$  is the magneto-electric coupling coefficient.

### 3. Simulation Results and Discussion

For performing simulations, the microwave studio package of CST simulation program has been used. Geometric and electrical properties of the slab cell in Fig. 1 are as follows. Lattice constants in respective directions of each cell are  $a_x = 5.0$  mm,  $a_y = 12.1$  mm, and  $a_z = 4.0$  mm. Besides,  $h = 3.1$  mm,  $g = 0.7$  mm,  $l = 2.0$  mm,  $d = 1.17$  mm. The substrate in each cell has the same geometry of lattice constants and has a loss-free relative permittivity with a value of 4.3. Perfect electric conductors with a thickness of  $50\mu\text{m}$  are utilized to imitate the response of metallic  $\pi$ -shaped inclusion and individual continuous wire of MM slabs to electromagnetic waves. Perfect electric and magnetic conductors are, respectively, assumed to be located over  $x-z$  and  $x-y$  planes to obtain the periodicity of the slab over  $y-z$  plane.

After obtaining the simulated S-parameters, we extracted  $n$ ,  $\varepsilon_y$ ,  $\mu_z$ , and  $\xi_0$  parameters. For example, Figs. 2 and 3, respectively, illustrate these parameters for various bi-anisotropic Composite MM slabs with  $w_1 = 0.1$  mm and  $w_1 = 1.2$  mm. From the dependencies in Figs. 2 and 3 we note the following results. First, it is seen that the value of magneto-electric coupling factor should not be omitted in the extraction of electromagnetic properties. Second, for the condition only when  $w_1 > w_2$  magnetic response of the Composite bi-anisotropic MM slab can change, while an increase in either  $w_1$  or  $w_2$  changes their electric response. Finally, an increase of  $w_2$  ( $w_1$  is constant) of our structure negligibly alters their electromagnetic response over the frequency region 4.49 GHz and  $f = 5.12$  GHz in which these slabs have right handed material property.

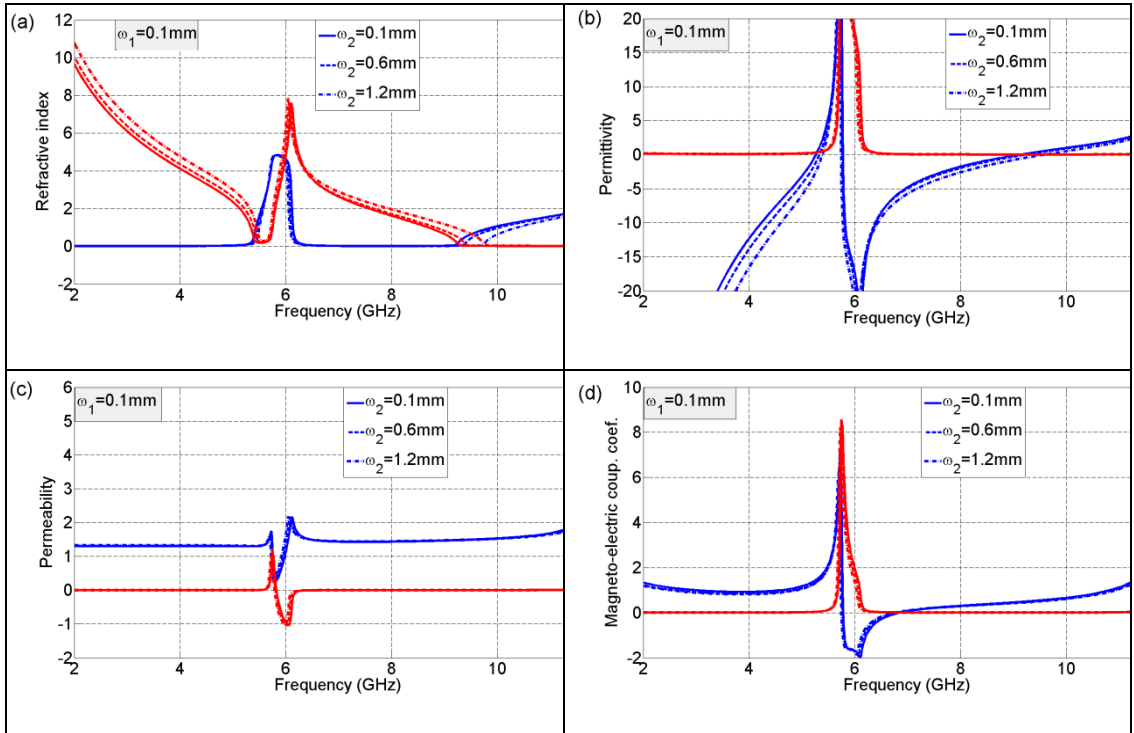


Fig. 2. Extracted electromagnetic properties of various bi-anisotropic Composite MM slabs with  $w_1 = 0.1$  mm.

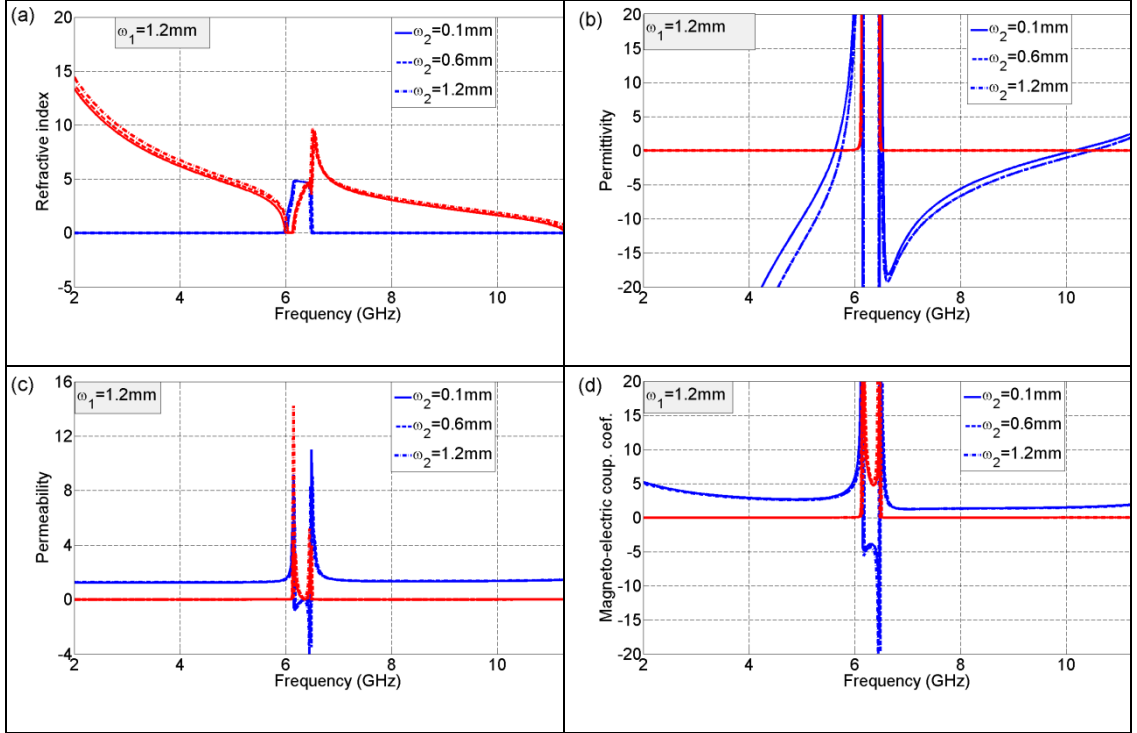


Fig. 3. Extracted electromagnetic properties of various bi-anisotropic Composite MM slabs with  $w_1 = 1.2$  mm.

#### 4. Conclusion

We have investigated effects of a change in width ( $w_1$ ) of constituent wire of a  $\pi$ -shaped bi-anisotropic MM slab and width ( $w_2$ ) of individual continuous wire of a Composite bi-anisotropic MM slab on their electromagnetic properties. After, we derived explicit expressions of (first) reflection coefficient and propagation factor in terms of simulated/measured S-parameters and then applied the phase unwrapping technique. From our investigation, we note the following key conclusions. First, we note that the value of magneto-electric coupling factor should not be omitted in the extraction of electromagnetic properties of  $\pi$ -shaped and Composite bi-anisotropic MM slabs especially for a frequency region in which measured/simulated S-parameters have significant changes. Second, a change in  $w_1$  importantly affects the electromagnetic response of  $\pi$ -shaped bi-anisotropic MM slabs over a frequency region in which these slabs possess right-handed material (RHM) property. Finally, while either  $w_1$  and  $w_2$  affects electric response of Composite bi-anisotropic MM slabs, only for the case  $w_1 > w_2$  changes magnetic response of these slabs.

#### References

- [1]. Choi M, Lee S H, Kim Y, Kang S B, Shin J, et al. 2011, Nature 470 369-73
- [2]. Barroso J J, Hasar U C 2012 J. Infrared Milli. Terahz Waves 33 237-44
- [3]. Hasar U C, Barroso J J, Sabah C, Kaya Y 2012 Prog. Electromagn. Res. 129 405-20